# Granular hydrodynamic study of non-spherical particles in a 3D fluidized bed

Jayaprakash, P.

*Award date:*
2016

Technische Universiteit Eindhoven University of Technology
Department of Chemistry and Chemical Engineering
Multiphase Reactors Group

# GRANULAR HYDRODYNAMIC STUDY OF NON-SPHERICAL PARTICLES IN A 3D FLUIDIZED BED

*Using Magnetic Particle Tracking Technique*

*Master thesis*

Pavithra Jayaprakash

Committee Members:
Prof. Dr. Ir. J.A.M.Kuipers
Prof. Dr. Ir. N.G.Deen
Dr. Ir. J.T.Padding
Dr. Ir. T.Noel
Ir. K.A.Buist

April 11, 2016

# Abstract

The large occurrences of non-spherical particles in industrial fluidized bed processes has inspired a great deal of attention towards understanding the behavior of these particles. This study, therefore, attempts to capture the granular hydrodynamics of non-spherical particles and compare them with the behavior of spheres. The experimental investigations are conducted in a laboratory scale 3 dimensional cylindrical fluidized bed using Magnetic Particle Tracking technique, which is a single particle tracking technique. With this technique, the particle's translational & rotational velocities, angular orientations & distributions and the local packing density in the bed are tracked. The influences of the inlet gas velocity, bed aspect ratio and particle aspect ratio are analysed and the results obtained showed that the non-sphericity of the particle influences the granular circulation pattern. The study also showed that the entanglement of the cylindrical particles in the bed, is found to affect several aspects of its hydrodynamics and that the orientation of these rods are a influenced not only by the gas velocity, but also by their radial position in the bed and the bed aspect ratio. It also showed that the rotational velocity of the cylinders are sensitive to the amount of particles in the bed. Significant differences between the behavior of spherical and non-spherical particles are realized in this research.

# Acknowledgements

This thesis would not have been possible without the help and support of the people around me and I would like to use this opportunity to sincerely thank them.

To begin with, I would like to thank Prof. Hans Kuipers for giving me this opportunity to work on this challenging yet inspiring and interesting topic. Not only did he fill our meetings with insightful discussions, he also took time to share some of his scientific experiences with me. This gave a personal touch to our meetings. The understanding and encouragement he showed, especially when I was still getting my equipment to work, kept me motivated throughout this endeavour.

It was during one of his lectures, in the first quartile, that I first heard Dr. Johan Padding, talk about non-spherical particles. He was excited to tell us, just how challenging they are and now to have actually worked with them and to have seen all the phenomena he taught us come to life is simply amazing. Johan's enthusiastic questions not only deepened my understanding of the topic but also made it more interesting and exciting for me to work with this project and I am truly grateful for that. I would also like to thank Dr. Timothy Noel for his genuine interest and out of the box questions, which gave a new perspective to my project.

A special and heartfelt thanks to my direct supervisor Kay Buist, who has been with me and guided me through all the ups and downs of this project. Since our introduction, Kay has always made sure he had time for me and has answered all my questions with a smile on his face, irrespective of the number of times I has asked them. Not only did he share my frustrations and excitements, but with his presence of mind and creative ideas, Kay has been a great support to me.

I am glad to have recieved help from Joost, Joris and Thijs for my experimental setup. A special thanks to Joris, for constantly coming up with ingenious solutions to get my setup working. He always made time for my requests and showed me that the workshop is a fun and interesting place! Although I never got a chance to work with Thijs's square column, I am sure it would be a success.

I would like to thank Lei Yang, for helping me with my TFM simulations and taking the time to teach me a few things about it and helping me understand how it works. I would also like to show my gratitude to Roland Gommers for helping me with my setup.

I would like to thank the SMR group that made me feel belonged and gave me a beautiful place to work. A special thanks to all my friends including Narayen, Maria, Sathya, Leander, Pradyumna, Marco and Lino for the wonderful times and memories they gave me and for taking time out of their busy schedule to vacuum along with me. Finally, I would like to thank my family for their constant support and for making all this possible.

# Contents

**Contents** vii

**List of Figures** ix

**List of Tables** xi

**1 Introduction** 1

**2 Literature Study** 3
- 2.1 Behavior of non-spherical particles . . . 3
  - 2.1.1 Flow-Field Methods . . . 5
  - 2.1.2 Particle Tracking Techniques . . . 5
- 2.2 Introduction to MPT . . . 7
- 2.3 Two Fluid Model . . . 8

**3 Experimental Procedure** 11
- 3.1 Experimental Setup . . . 11
- 3.2 Material Used . . . 12
- 3.3 Experimental Procedure and Post Processing . . . 13

**4 Results and Discussions** 15
- 4.1 Determination of $u_{mf}$ . . . 15
- 4.2 MPT Experiments . . . 17
  - 4.2.1 Strengths of MPT . . . 18
  - 4.2.2 Effect of superficial velocity . . . 23
  - 4.2.3 Effect of Bed Height . . . 29
  - 4.2.4 Effect of Aspect ratio of Particle . . . 31
- 4.3 TFM vs Experimental results . . . 32

**5 Conclusions** 37

**6 Recommendations** 39

**Bibliography** 40

**Appendix** 45

**A Supporting Studies** 45
- A.1 Estimation of void fraction for different aspect ratio particles . . . 45
- A.2 Calculation of $u_{mf}$ . . . 45
- A.3 Effect of Helmholtz coil . . . 46
- A.4 Velocity Profiles for 2.25 aspect ratio rods . . . 47

# List of Figures


2.1 Pressure regions surrounding a 2D non spherical particle of various orientations in a flow regime . . . 4
2.2 The magnetic field exerted by a dipole magnet on a sensor with respect to the sensor's position and orientation . . . 8

3.1 Experimental Setup . . . 11
3.2 Bed Material . . . 12

4.1 Pressure drop studies . . . 16
4.2 Check for Preferential Flow . . . 18
4.3 Cylindrical Representation . . . 18
4.4 Azimuthally averaged occupancy plot . . . 19
4.5 Linear velocity profile at a excess velocity of 1.5m/s . . . 20
4.6 Rotational velocities at excess gas velocity of 1.5m/s . . . 21
4.7 Representation of $\theta$ and $\varphi$ . . . 22
4.8 Behavior of $\theta$ at excess velocity of 1.5m/s . . . 22
4.9 Behavior of $\varphi$ at excess velocity of 1.5m/s . . . 23
4.10 Behavior of spherical particles (aspect ratio=1) for various excess gas velocities . 24
4.11 Behavior of 4.5 aspect ratio rod mixture for various excess gas velocities . . . 25
4.12 Rotational velocity along the radial direction for various excess gas velocities . . 27
4.13 Rotational Velocity behavior of spheres and 4.5 aspect ratio rods . . . 28
4.14 Virtual particle concentration . . . 28
4.15 Velocity profile comparison at $u_{excess}$ 1.5m/s . . . 29
4.16 Distribution of $\theta$ at $u_{excess}$ 1.5m/s . . . 30
4.17 Height averaged linear velocity profile along the r for the different particles . . . 30
4.18 Rotational velocity profile along the r for the different particles . . . 31
4.19 Average $\theta$ along the r for the different particles . . . 32
4.20 Velocity profiles of Spheres (aspect ratio=1) for excess velocity of 1.5m/s . . . 33
4.21 Velocity profiles of small rods (aspect ratio=2.25) for excess velocity of 1.5m/s . 33
4.22 Velocity profiles of intermediate rods (aspect ratio=4.5) for excess velocity of 1.5m/s . . . 34
4.23 Velocity profiles predicted by TFM for intermediate rods (aspect ratio=4.5) . . . 35

A.1 Porosity of bed for different aspect ratio particles . . . 45
A.2 Effect of Helmholtz coils for spheres . . . 46
A.3 Linear velocity profiles . . . 47

# List of Tables

3.1 List of geometric configurations and sphericity of the particles . . . . . 12
3.2 Relevant properties of the experimental setup . . . . . 13

4.1 Minimum fluidization velocities of the various aspect ratio particles . . . . . 17
4.2 Grid specification . . . . . 19

# Chapter 1

# Introduction

**Need to track non-spherical particles in a fluidized bed setup**

Possessing favorable properties that include intense solid mixing, large gas-solid contacting regions and enhanced mass and heat transfer characteristics, has made gas-solid fluidization become an integral part of multiphase operations. Additionally, they provide the possibility of continuous and large scale operations, thus establishing their importance in the industrial scale. This combined with their complex multiphase flow dynamics has initiated several intense studies, both experimentally and computationally, in order to derive a better understanding of the granular motion occurring within these beds. A good knowledge of its behavior is essential for the design, optimization and control of these processes.

Although certain computational models have had great success in capturing its full range of dynamics, many however assume a spherical geometry and near elastic behavior for the particles[1]. This assumption is highly convenient owing to its simplicity, the fact that the behavior of spheres is well understood and the availability of numerous models to describe the solid phase interaction with the fluid. Moreover spheres can be described by just one characteristic value namely its diameter, whereas non-spherical particles require several parameters. Even very regular shapes, like ellipsoids or fibers, require at least two parameters to describe them.

All these attributes may make the use of spherical particles highly attractive but nevertheless, in reality the solid phase encountered is *rarely ideal and frequently non spherical*. Common fluidized bed processes such as catalysis, pyrolysis, gasifications and so on, often deal with particles that are non spherical and have aspect ratios that are larger than 3. Some examples include, the use of flaky or stalk-like biomass particles in gasifiers and combustors, the drying of pills in fluidized beds and the moisture content adjustment of cut-tobacco and so on. In order to improve the quality of these processes, a detailed understanding its granular behavior is necessary.

However atempting to study these non-spherical particles using equivalent volume spheres is not the solution to it. This is because the study of flow with non-spherical particles is considerably more complicated than flows with spherical particles. Where a sphere experiences mainly drag force, a non-spherical particle is significantly affected, in addition, by the transverse lift force, pitching torque and a counter-rotational torque. All these components acting on a non-spherical body depend not only on the Reynolds number, but also on the angles made between the axes of the particle and the direction of the incoming flow, as high aspect ratio particles can have varying orientation with respect to the flow[2]. Unlike in the case of spheres, the collisions now occurring are also affected by the orientations of the colliding particles and the aforementioned altered forces. The altered drag and collision characteristics, in turn influence the voids and heterogeneous structures, as well as mass and heat transfer rates.

Most often the effects of non-sphericity is addressed by incorporating a Sphericity Factor $\Phi$, which although may yield promising results, it is nonetheless far from describing the actual behavior of the non-spherical solid[3]. This is especially the case in dense systems where multiple simultaneous particle contacts cannot be ignored and as such the effects of angular orientation and particle rotation become exceedingly influential in describing the behavior of the solid phase. For instance, Cai et al[4] suggest that, when compared to a sphere, the force and movement of a cylindrical particles in a flow field is often affected by the orientation of the particle. Zitoun et al[5] have presented results to suggest that objects with high aspect ratios tend to align to the flow, within constraints set by solid concentration, and that elongated solids may rotate until an equilibrium position is achieved. Such orientational behavior of the particles influence the process quality and the fluidizing nature of the system[6][7]. Authors including Hilton and Cleary[8][9][10] have stressed that particle shape is a crucial factor that influences several aspects of the hydrodynamics including pressure drop, local solid porosity and so on. In spite of their significance there are very few studies on non-spherical particles in a fluidized bed.

Particle rotation is yet another influential parameter that need to be taken into account while considering granular hydrodynamics. Several authours have stressed the influence particle rotation has on the granular motion, especially for densly packed systems. For example, Wang et al [14] highlights the importance of rotational motion of particle by showing that it plays a vital role in defining its heat transfer coefficients. Even for the simplest of particle shapes - spheres, Goldsmith[11] has shown that that ignoring the particle rotation causes a major deficiency in the multi-fluid models, in contrast to discrete particle models which provide closer resemblance to the experimental results.*It therefore, becomes highly advantageous to experimentally track a non-spherical particle under fluidized conditions and attempt to completely understand several aspects of its behavior.*

Although several studies are available on fluidized beds, throughout literature, most however are limited to 2Dimensional or pseudo-2D systems in which the particles motion is restricted by the front and back walls. 3Dimentional studies are rarer to come by and this is owed to the fact that they poses several challenges both numerically and experimentally. Numerically because of the requirement of the high computational costs and experimentally because of the difficulty to visualize the flow and record measurements. However authors such as Cranfield and Geldart $\big(1974\big)$ have since proved that there exist significant difference in the behaviors of a pseudo-2D and full 3D systems. Fortunately a recently introduced novel Magnetic Particle Tracking technique, has the ability to make up for this shortage by allowing the measurements in a 3D system. Since it is clear that geometry of the system has a profound influence on the behavior of the fluidized bed and because the most commonly used geometry in industry is a cylindrical one, this thesis studies the effects of non-sphericity of the particles in a full 3D cylindrical fluidized bed.

# Chapter 2

# Literature Study

## 2.1 Behavior of non-spherical particles

Large, non spherical particles are of special interest as they are involved in processes such as refuse-derived fuel, food processing, bulk handling of processed solids, sterilization of biomaterial and so on. These large particles, fall under the Geldart D particle classification and the typical behavior of Geldart D particles[12] include:

1. Rapidly coalescing bubbles that grow to large size
2. Low dense phase voidage
3. Enormous requirement of gas for fluidization these solids
4. Slugging of particles, especially at the onset of fluidization
5. Transition to turbulent flow occurs at lower relative velocity
6. Operates at the churning fluidization regime at high velocities
7. Prone to severe channeling behavior

In addition to the above listed properties, the non sphericity of these particles also plays a role in defining its behavior in the fluidized bed. Thus capturing the behavior of these particles have become an object of interest to several researchers and recently, both experimental and computational studies, involving them are being attempted. DNS simulations of non-spherical particles suggest that the interaction of these particles with a fluid flow is a complex phenomenon even for axisymmetric particles in a uniform flow. It has been shown that the shape of the solid has a great influence on the behavior of the particle, not only by changing the values of the experienced forces and torques but also by shifting the Reynolds number at which the transition to unsteady flow occurs[3].

Analytically it has also been indicated that the dynamics of a non-spherical particle immersed in a random axisymmetric flow exhibits four regimes including the rotation around the axis of symmetry of the flow, tumbling, a combination of rotation and tumbling, and preferential alignment with a direction oblique to the axis of symmetry of the flow. This regime is selected by the form of the anisotropic component of the flow and by the geometrical shape of the particle[13]. Also it has been observed that non-spherical particles try to locally maximize their drag, although the inertia of the particles and the local fluid velocity fluctuations and gradients prevent this from occurring instantaneously. Fig 2.1 shows the pressure regions surrounding a 2D non spherical particle of various orientations in a flow regime[14]. High pressure regions on the acute sides of a non-spherical particle result in a torque and thus the particle is most

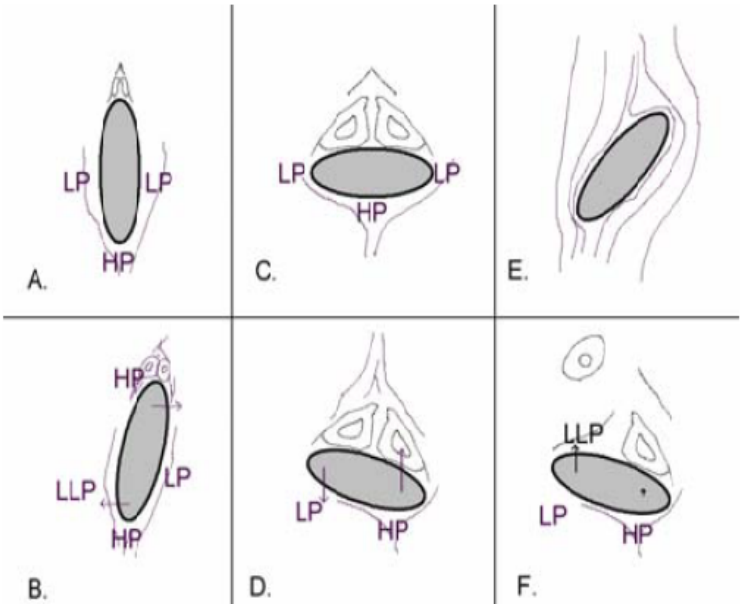


Figure 2.1: Pressure regions surrounding a 2D non spherical particle of various orientations in a flow regime

stable when the axis of the particle is perpendicular to the local direction of the flow i.e. there is zero torque on the particle when its longest axis is aligned perpendicular to the flow. This stable alignment causes the non-spherical particles to have a larger average velocity compared to spherical particles with the same equivalent diameter and thus move considerably faster through the channel. Oscillation of the particle about its axis has also been reported.

Particles always rotate when moving along the flow due to the non-homogeneous flow field and particle collisions. According to the Magnus Effect, a lift force will be produced by its rotation, which in turn changes the moving trajectory of the particle in the flow. This lift force is rather significant whereby the behavior of the solid phase and flow fields are influenced by it. For instance, Yuan et al showed that the voidage inside the fluidized bed was enlarged due to particle rotation and from Wang et al[15] it can be understood that the particle rotation plays a significant role in heat transfer of the particles. It has been experimentally seen that the average rotational speed of spherical decreases with the increase in particle size and that this speed is more pronounced in irregular shaped particles[16]. Additionally the wall roughness that usually affects the translational velocity in the case of a sphere, now seems to play a more dominant effect by inducing additional rotational characteristics in a non-spherical particle[2].

Thus ignoring the effects of particle shape, rotation and orientation would undoubtedly produce results that are too idealized to provide a quantitatively accurate prediction of the hydrodynamics. However there is not enough experimental data to completely validate the above mentioned effects, mainly owing to the difficulty in capturing these characteristics of the solid phase. But recent advancements in technology and computational power, has given birth to techniques that are capable of capturing the particles behavior on a highly detailed level.

Among them the *noninvasive techniques*, as opposed to the techniques that involve probes which cause local disturbances in the bed, have shown great potential in the validation of detailed computational models and in characterization of dense granular flow. These techniques include *Flow field investigation* and *Particle tracking* techniques:

### 2.1.1 Flow-Field Methods

1. **Particle Image Velocimetry (PIV)** is a commonly employed technique where a high-speed CCD camera is used to record images of the particles in the illuminated front plane. Two subsequent images of the flow, separated by a short time delay, $\Delta t$, are divided into small interrogation areas. Cross-correlation analysis is used to determine the volume-averaged displacement of the particle images between the interrogation areas in the first and second image. The advantage of PIV is that an entire velocity vector field, also of very small particles, can be obtained non-intrusively. Moreover, time-averaged velocity fields and also turbulent quantities can be determined by recording many consecutive images. Another advantage is that both very low and very high (sonic speed) particle velocities are measurable. A drawback of PIV is that only close-wall velocity vector fields can be detected and wall effects may have an impact on the measurement in small apparatuses. Single particle trajectories are also not measurable because an insight in the third dimension is not possible.

2. **Electrical Capacitance tomography (ECT)** is used to determine local particle concentration and velocities, by making use of the variation in the dielectric capacity depending on solid concentrations. If the measurement is done in two closely sequenced points along the direction of flow, the particle velocity is accessible by cross-correlation of two signals. Although the technique is simple and cost efficient, it is incapable of capturing 3D particle trajectories. Moreover their results are severely influenced by electrostatic interferences and the properties of the solids, especially their moisture contents[6].

3. **Magnetic resonance tomography (MRT)**, uses the effect of nuclear spin of the hydrogen nuclei on the magnetism. A coil around the system applies a strong magnetic field whereby the hydrogen nuclei are aligned. A radio wave field with high frequency effects the deflection of the current alignment and the onset of a swaying motion. This so-called cross magnetization is a function of the position and can be measured through the current induced in the coil, whereby the particle position is assessable. The advantage of this method is that the spatial resolution is very high. However this method is very expensive and it is necessary that hydrogen nuclei are present in the used material. Also it is not possible to follow a single particle and the current measurable fluidized bed is only 50 mm[17].

### 2.1.2 Particle Tracking Techniques

1. **Phosphorescence measurement**an optical particle tracking technique. Brewster and Seader[18] developed this tagging method for measuring particle residence times in industrial pneumatic transport systems. The particles are coated with powdered phosphorescent pigment using glue, illuminated with light over an extended period, and subsequently injected using a high pressure pulse of air. The tracer particles are detected using a series of photomultiplier tubes (PMTs) located downstream. Although this technique is highly cost effect, its major disadvantage lies in the fact that it can account only for the residence time distribution and velocity between specified positions, but no detailed information, on the particles or their trajectories, can be obtained[19][20].

2. **Fluorescent technique** is yet another optical method that also requires low investment and easy handling. But unlike the phosphorescence studies this technique can track a single particle and can provide more detailed information on particle trajectories. In this case the marker particles are contacted with an optical whiting substance (Fluorescent Brightener 28) and fluorescence under a UV light[6]. These particles are then tracked with a high speed video camera employing optical filters whose fluorescent wavelength is

matched to that of the markers. Image analysis is then used to obtain particle trajectories and velocities as a result of interaction behavior. Apart from preconditioning of the marker particles and using transparent walled apparatus, the accuracy of the tracking algorithm is dependent on the noise, position of imaging array, shape of particle and spatial resolution of imaging. These algorithms are often subjected to both determinate and indeterminate errors[21].

3. **Particle Tracking Velocimetry (PTV)**, that proceeds by taking images of the particle at different times and calculating the particles velocity based on the particles displacement in subsequent images. In general a 3D-PTV consists of three or four cameras that are in an angular configuration. The diffracted light from the flow tracers in the measured medium is recorded synchronously. The flow is illuminated by a laser or another light source. A fluorescent or diffractive particle can be used as the tracer. With this technique, particle concentrations, particle linear and angular velocity distribution of even very small grains can be determined. It requires low initial costs and simple operational procedure. However the tracer particles need to be pretreated in order to emit light and the walls of the system need to be transparent[5][19][22].

4. **Positron emission particle tracking (PEPT)**, which belongs to the family of radioactive measuring techniques. PEPT uses a class of radioisotopes, which decay through the emission of positrons. When these positrons encounter an electron, they emit back to back gamma rays. The particle position can then be determined by calculating the intersection of the emitted gamma rays, which can be detected. Using PEPT, a single tracer particle can be accurately tracked as it moves within the field of view of the positron camera. Although this technique has high spatial resolution, they are expensive, involve dangerous radiation, have plenty of runaway values and require preconditioning. All these factors make PEPT an expensive technique[6][23].

5. **Computer Aided Radioactive particle tracking (CARPT)** is yet another technique based on radioactive isotopes used in order to study the particle trajectory. It is able to provide 3D information of a particle by continuously monitoring the gamma rays emitted by the tracer, which are captured by strategically located scintillation detectors. The attenuation of the radiation is used to estimate the position of the particle. Using the Lagrangian particle velocities, ensemble averaging is performed to calculate the average velocities and various velocity-related quantities. The reliability and accuracy of the CARPT measurement largely depends on several key factors, which include the tracer particle selection, calibration of the detectors and signal processing. The issues regarding the calibration and the tracer particle have been discussed in detail by Degaleesan et al., Kumar et al. and Larachi et al [25-28].

6. **Infrared Thermography facilitated by microwave heating** is a technique to capture the particle trajectories and thereby studying cycle-time and resident-time distribution. In this technique an infrared imaging camera is used to detect the electromagnetic energy radiated by the polar tracer that is heated consecutively by a microwave. This signal is converted it into an electronic video signal. The microwave heating technology is based on the transformation of alternating electromagnetic field energy into thermal energy by affecting the polar molecules of a material. Thus a single polar tracer is tracked and extended time series of the actual path of a polar tracer are measured for a fixed time to obtain the particle trajectories. Advantages of the technique includes the ability to obtain the entire concentration field directly, volumetric and selective heating, compactness of equipment, speed of switching on and off, and pollution-free environment[16][17].

7. **Magnetic Particle Tracking (MPT)**is a recently introduced promising particle tracking technique that uses a small magnetic source as the tracer particle. The magnetic signal

of the tracer is detected by a multitude of sensors placed around the fluidized bed under study. Data from these sensors are used to reconstruct the magnetic field and thereby the position, linear and angular momentum fluxes and orientational order of the particle can be determined. The main advantage of the MPT technique lies in the fact that they are 3D compatible and possess relatively low initial cost and simpler/safer handling especially when compared to the techniques involving radioactive tracers[24]. However the field strength measured at the sensor depends heavily on the strength of the magnetic marker, its relative orientation to the sensors and its distance to the sensors. This ability of MPT to measure the orientation of the particle with respect to the sensor, aids in the study of rotational behavior of the particle, which plays a vital role especially in the understanding of non-spherical particle behavior. Buist et al[25] have not just provided a detailed account of the working principle of MPT but have also shown that the MPT in combination with SQP (Sequential Quadratic Programing) algorithm and wavelet filtering and Particle Image Velocimetry in combination with Digital Image analysis (PIV-DIA) compare very well quantitatively.

Since this study focuses on tracking granular motion of non-spherical particle, it is not sufficient to just track the position and translation velocity of the particle but also to capture its orientation and rotational behavior during fluidization. Therefore from the above comparison of the different techniques, MPT technique seems to be the most suited technique to study the current scenario.

## 2.2 Introduction to MPT

MPT was first used in research to track a pill through the digestive system by Stathopoulos et al[26]. Mohs et al[6] used this technique to monitor a single particle in a spouted bed. MPT is based on the analysis of a quasi-static magnetic field around the magnetic marker. Considering the magnetic moment of the tracer is known, the system has five degrees of freedom that include the position of the marker characterized by x, y, and z axes and angular placement of the tracer provided by $\theta$ and $\varphi$. This property deems that at least five sensors are necessary to precisely determine the location and the orientation of the tracer particle. The magnetic signal of the tracer is captured by a series of anisotropic magneto-resistive (AMR) sensors placed around the fluidized bed. The quasi static magnetic field induced by the magnetic tracer is given by Eq 2.1.

$$\overline{H}\left(\overline{e_p}, \overline{r_{ps}}\right) = \frac{1}{4\pi}\left(-\frac{\mu_m \overline{e_p}}{\mid \overline{r_{ps}} \mid^3} + \frac{3\mu_m \left(\overline{e_p} \cdot \overline{r_{ps}}\right)\overline{r_{ps}}}{\mid \overline{r_{ps}} \mid^5}\right) \tag{2.1}$$

Where $\overline{r_{ps}}$ is the relative distance of the tracer particle to the sensor, $\mu_m$ is the magnetic moment of the tracer particle, and $\overline{e_p}$ is the orientation unit vector of the magnet, calculated via a transformation of the angles $\theta$ and $\phi$ from the spherical to the Cartesian coordinate system. From figure 2.2 it can be seen that the magnetic field obtained from 2.1 cannot be directly used to estimate the strength of the field as the signal measured by the sensor is highly dependent on the orientation of the sensors themselves. Thus the sensor output St is given as a product of the magnetic field $\overline{H}$ and the sensors orientation in the field $\overline{e_s}$ as shown in Eq 2.2. Evaluation of the field by taking the sensor position and orientation into account results in providing an estimate of the tracers position and orientation.

$$S_t = \overline{H}\left(\overline{e_p}, \overline{r_{ps}}\right) \cdot \overline{e_s} \tag{2.2}$$

Because it is possible to measure the orientation of the tracer particle, it is also possible to measure a relative change in the orientation, and thus the rotational velocity of the particle

can be calculated. This is not possible with most measuring techniques and is therefore a big advantage of MPT. The whole setup including the sensors are placed within a region surrounded by an Helmholtz coil, used to neutralizes the magnetic field of the earth in the measuring area to provide unbiased results.

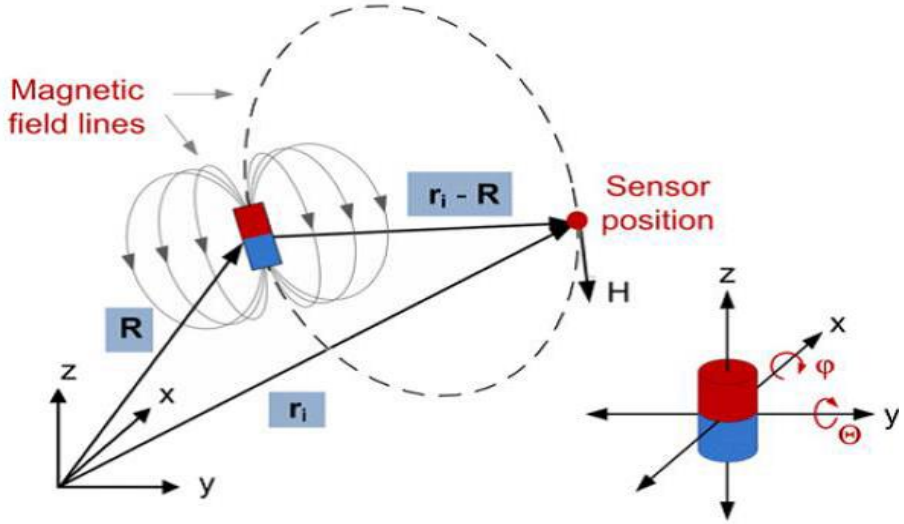


Figure 2.2: The magnetic field exerted by a dipole magnet on a sensor with respect to the sensor's position and orientation

An optimization technique is used to estimate the most probable position and orientation of the tracer by comparing the measured and theoretical magnetic field strengths, at the different sensors. This is be done by solving a minimizing function, shown in 2.3, which is corrected for the standard deviation in individual sensors, in order to ensure the less accurate sensors have less influence.

$$P_i = erf\left(\frac{\mid (S_{m,i} - \langle S_m \rangle) - (S_{t,i} - \langle S_t \rangle) \mid}{\sqrt{2}\sigma_{S_{m,i}}}\right) \tag{2.3}$$

All chances are summed and divided by the number of sensors. Thus Q, from Eq 2.4, is a value between zero and one which provides the probability of finding the tracer at a certain position x, y, z, with $\theta$ and $\phi$ orientation.

$$Q = 1 - \frac{\sqrt{\sum P_i^2}}{N} \tag{2.4}$$

The main advantage is that this function is more accurate and simpler than the quality function, as it estimates average of all the probabilities of finding $S_{t,i}$ given $S_{m,i}$ and $\sigma_{S_{m,i}}$, [25]

## 2.3 Two Fluid Model

As experimental investigations at industrial scale are costly and even at laboratory scale the study of dense two phase systems are quite a challenge, thus simulations that can predict fluidization behavior are of high value not only academically but also industrially. However, since the number of particles involved in most practically gas-solid flows are extremely large, thus impractical to solve the equations of motion for each particle. It is, therefore, advantageous to investigate particulate flows in large process units with models that use averaged equations of motion such as the **Two Fluid Model (TFM)**.

In TFM, the gas phase is described by using the volume averaged Navier-Stokes equation

$$\frac{\partial\left(\epsilon_f \rho_f\right)}{\partial t} + \nabla \cdot \epsilon_f \rho_f \overline{u} = 0 \tag{2.5}$$

$$\frac{\partial\left(\epsilon_f \rho_f \overline{u}\right)}{\partial t} + \nabla \cdot \epsilon_f \rho_f \overline{uu} = -\epsilon_f \nabla p - \nabla \cdot \left(\epsilon_f \overline{\overline{\tau_f}}\right) + \overline{S_p} + \epsilon_f \rho_f \overline{g} \tag{2.6}$$

Where, $\overline{S_p}$ is the source term accounting for particle fluid momentum exchange i.e. drag. The speciality of TFM lies in the fact that it treats the solids also as a second fluid, fully interpenetrating the gas phase. At present, the most advanced CFD model used for industrial-scale reactors is the two-fluid model coupled with the kinetic theory of granular flow (KTGF). In order to describe the solid phase using a continuum model, it is essential to be able to describe the collisions occurring between particles in the particulate phase and it is for this reason that the KTGF was introduced, as KTGF provides the particle phase properties. This approach requires TFM to make several assumptions regarding the particle-fluid and particle-particle interactions, including the premises that (i) the velocities of the particles are Maxwell-Boltzmann distributed, (ii) collisions are only slightly inelastic and described by a constant coefficient of restitution and (iii) that the particle-fluid interaction is governed by a drag model interpenetrating the gas phase. Separate equations for the mass and momentum balances have been used. Eq 2.7 describes the momentum balance.

$$\frac{\partial\left(\epsilon_s \rho_s \overline{v}\right)}{\partial t} + \nabla \cdot \epsilon_s \rho_s \overline{vv} = -\nabla \cdot \left(P_s \overline{I} + \epsilon_s \overline{\overline{\tau_s}}\right) + \epsilon_s \rho_s g - S_p - \epsilon_s \nabla P_f \tag{2.7}$$

To close the solid pressure and stress terms an extra equation for granular flow temperature of the solid phase is solved, which follows from KTGF, shown by Eq 2.8

$$\frac{3}{2}\left[\frac{\partial\left(\epsilon_s \rho_s \theta_t\right)}{\partial t} + \nabla \cdot \left(\epsilon_s \rho_s \overline{\nu} \theta_t\right)\right] = -\nabla \overline{\nu} : \left(P_s \overline{I} + \epsilon_s \overline{\overline{\tau_s}}\right) - \epsilon_s \nabla \cdot \left(-\kappa_t \nabla \theta_t\right) - \gamma_t - 3\beta_A \theta_t \tag{2.8}$$

However studies have shown that the comparison of TFM with DEM results demonstrates that modelling the particulate phase using an ideal KTGF does not accurately represent the fluidization behavior and these errors were attributed to the fact that KTGF is limited to slightly inelastic spherical particles and does not account for rotational friction effects. Goldschmidt et al showed that the absence of rotation is a deficiency of the model [11][27]. Some authors including Lu et al[27] have shown that by introducing an apparent coefficient of restitution to account for rotation of particle, TFM simulations of the voidage and time-averaged particle velocity have better agreement with the experimental and DEM simulation results. Yang et al[28] has added a balance for the rotational granular temperature and respective closure shown in Eq 2.9

$$\frac{3}{2}\left[\frac{\partial\left(\epsilon_s \rho_s \theta_r\right)}{\partial t} + \nabla \cdot \left(\epsilon_s \rho_s \overline{\nu_s} \theta_r\right)\right] = -\epsilon_s \nabla \cdot \left(-\kappa_{r1}\right) \nabla \theta_r - \kappa_{r2} \nabla \theta_t\right) - \gamma_t \tag{2.9}$$

However this theory is still in progress and as an initial step there are two assumptions made. These are (i) the mean rotational velocity is zero and (ii) the walls of the system are adiabatic i.e. gradient of rotational granular temperature at the wall is taken as zero.

# Chapter 3

# Experimental Procedure

This chapter briefly describes the experimental setup, the materials used and the post processing procedure required for MPT technique.

## 3.1 Experimental Setup

For this research a 3 dimensional cylindrical column with inner diameter of 0.174 m and height 1 m is used. The column is surrounded by a sensor array consisting of 72 sensors divided among 4 ringed structure of 26cm diameter each, shown in fig 3.1a. These ringed structure are placed 15 apart from each other in height thus making the total height of the sensor array 45 cm. The sensors measure the magnetic field emitted by the magnetic tracer particle at the rate of 1 KHz and the measurements are sampled to 50Hz.

A mass flow controller, with a capacity of 500 $Nm^3$/h, is used to control the velocity of the fluid phase. The base of the column is provided with a conical distributing chamber, completely filled with glass particles of 3mm. The purpose of this chamber is to evenly distribute the incoming fluid, so as to effectively circumvent the problem of preferential flow that otherwise occurs either because of the bend in the inlet air-hose or due to the poor distribution of distributor plates. The distributing chamber is covered with a *distributor plate*. The distributor plate used is 3mm

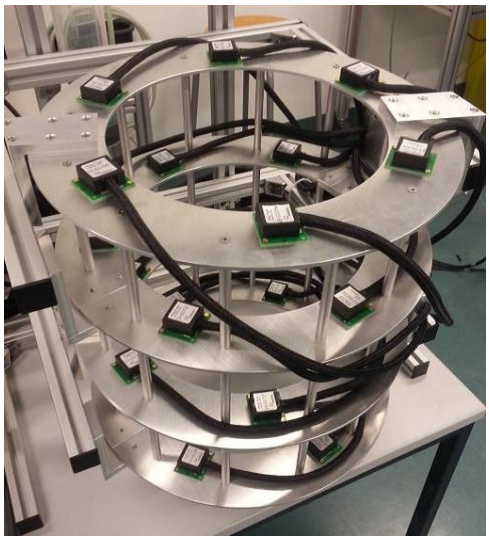

(a) Sensor Array

(b) Fluidized Bed placed inside a Helmholtz coil

Figure 3.1: Experimental Setup

thick, Brass plate with an open area of 20.3 %. It is vital to ensure that all the components in

the vicinity of the sensor array, such as the distributor plate, the bolts and nuts and so on are nonmagnetic and non-magnetizable. A *differential pressure sensor* of 1 bar capacity, measuring at a frequency of 10 Hz, is inserted at the base of the column just above the distributor plate. A Labview software is used to record the pressure changes as a function of time.

Helmholtz coil, through which an electric current is passed, is configured in such a way that it neutralizes the earths magnetic field at its center. A magnetometer is used to determine this configuration of the coil. As shown in fig 3.1b, the fluidizing column along with its sensor array are placed in the middle of the Helmholtz coil, so that the magnetic tracer will be unbiased by the earths magnetism.

## 3.2 Material Used

This study focuses on the difference in granular hydrodynamics based on the difference in particle shape quantified by their aspect ratio(AR). Thus, cylindrical particles with varying aspect ratios have been selected, and their granular behavior is compared to that of spherical particles with equivalent diameter. The geometrical configuration and sphericity of the different aspect ratio particles are listed in the Table 3.1

| **Name** | **Dimensions (mm)** | **Aspect Ratio(AR)** | **Sphericity (Φ)** |
|---|---|---|---|
| Sphere | 3.0 | 1 | 1.00 |
| Small Rods | 2.0 x 4.5 | 2.25 | 0.818 |
| Intermediate Rods | 1.6 x 7.0 | 4.5 | 0.719 |
| Long Rods | 1.2 x 12 | 10 | 0.579 |

Table 3.1: List of geometric configurations and sphericity of the particles

The **Tracers** used are Neodymium magnet with an equivalent spherical diameter of 3mm emitting a magnetic field of 0.014 H. Any tracer smaller, would compromise the accuracy of the sensor measurement as it would have a very low magnetic field associated with it. In order to ensure that the bulk particles and the tracer behave similarly, it is vital to select a material that has a density that is comparable to the density of the tracer material. Thus austenitic stainless steel (SS 300 series) is selected. These particles are then annealed at a temperature of 780°C to render them non-magnetizable. The annealed particles are shown in fig 3.2a and 3.2b. These particle belong to Geldart D classification. All the relevant properties of the system are provided in Table 3.2

(a) Annealed spheres (Aspect Ratio:1)

(b) Annealed long rods (Aspect Ratio:10)

Figure 3.2: Bed Material

| | |
|---|---|
| **3D Fluidized Bed** | |
| Inner Diameter | 0.174 m |
| Height | 1 m |
| Scaffold | Aluminum |
| Distributor plate | Brass |
| Distributor thickness | 3 mm |
| Pore size | 0.9 mm |
| Open area | 20.3 % |
| Inlet Air tube | Perspex |
| Max possible superficial velocity | 6.5 m/s |
| Max flow rate | 500 $Nm^3$/h |
| **MPT Sensor array** | |
| Sensor type | Tri-axes AMR |
| Frequency | 1 KHz |
| Height | 0.45 m |
| Diameter | 0.26 m |
| Number of sensors | 4 * 18 |
| **Tracer** | |
| Material | Neodymium |
| Equivalent Spherical Diameter | 3 mm |
| Density | 7.3 g/$cm^3$ |
| Magnetic moment | 0.014 $Am^2$ |
| **Particles** | |
| Material | austenitic stainless steel |
| Density | 7.87 g/$cm^3$ |
| Equivalent Spherical Diameter | 3 mm |

Table 3.2: Relevant properties of the experimental setup

## 3.3 Experimental Procedure and Post Processing

For the fluidization experiments, the initial volume of the bed is maintained a constant for the different aspect ratio particles. Since the shape of the particle influences the porosity of the bed, a simple study is done to determine the bed voidage corresponding to the various aspect ratio particles. This study is shown in Appendix A.1.

To begin with, pressure drop studies are conducted in order to determine the minimum fluidization velocity ($u_{mf}$) corresponding to the different aspect ratio particles. Once the $u_{mf}$ of the particles are measured, the different systems are analysed and compared for constant excess gas velocities, i.e. $u_{excess} = u - u_{mf}$. Each Fluidization experiment is conducted for a period of 3 hours.

The collected data is sampled at 50Hz and signal filtering, using a *wavelet filter*, is done to suppress the high noise levels and to produce a smoother signal data that increases the accuracy of the optimizing algorithm. Buist et al[25] has already shown the superiority of nonlinear optimization algorithms, especially highlighting the strength of the *SQP(sequential quadratic programming)* algorithm for the MPT technique. Since the effectiveness of any algorithm can be improved by providing as much information as possible, the physical boundaries of the 3D setup and the bounds of the orientation unit vectors of the tracer are provided as the constraints

of optimization. These constraints are shown in 3.1.

$$\begin{aligned} \sqrt{x^2 + y^2} &\leq \frac{D}{2} \\ -\frac{H}{2} \leq Z &\leq \frac{H}{2} \\ |\,\overline{e_p}\,| &= 1 \\ -1 \leq e_x &\leq 1 \\ -1 \leq e_y &\leq 1 \\ -1 \leq e_z &\leq 1 \end{aligned} \tag{3.1}$$

All gradient-search methods, including SQP algorithm, need an initial guess-value to converge to a minimum. Thus to begin optimization, the algorithm is initialized using a *multi-start method*, i.e. multiple initial guesses are given to solve for the first time step. Using these guess values, the global minimum of the system is found. For the following time steps, the solution of the previous time step is considered as the initial estimate and local minima are estimated. Unfortunately the algorithm is not always converging or the quality function is sometimes too high. In those cases, the algorithm is set to reinitialize. Also, when the algorithm finds a minimum on the boundary constraint of the setup, the algorithm is set to reinitialize, as the solution in that case would be is physically impossible.

# Chapter 4

# Results and Discussions

The results obtained from this study are discussed in this chapter. The strengths of the Magnetic Particle Tracking technique are highlighted and the differences in granular hydrodynamics of the different aspect ratio particles are investigated.

## 4.1 Determination of $u_{mf}$

The pressure drop is plotted as a function of velocity and it is seen that all the different aspect-ratio particle systems tend to follow the predicted pattern, according to which, at relatively low gas flow rates the increase in pressure drop is proportional to the gas velocity until it reaches a certain pressure drop, $\triangle p_{max}$. This point corresponds to the minimum fluidization velocity of the system and at this point the bed unlocks. For any further increase in the velocity the pressure drop should remain practically unchanged.

Fig 4.1a shows that in the case of spheres, not only is the predicted trend obeyed but it is also seen that the pressure drop curve is retraceable when the velocity is decreased from any point above $u_{mf}$. Thus effectively having a single $u_{mf}$ value. The minimum fluidization velocity is estimated to be 2.81 m/s and this value coincides with the theoretical predicted $u_{mf}$ of 2.77m/s (calculation shown in Appendix A.2).

In the case of the Long rods (AR=10), fluidization is not possible for the current range of the mass flow controller owing to the severe channeling of the bed. At relatively high flow rates, particles in the channel tend to be spouted out from the channels, while the bulk of the bed remains stationary. Owing to this characteristic, these particles are not investigated further.

In the case of Intermediate rods (AR=4.5), although fluidization is possible, channeling of the bed beyond minimum fluidization was observed. This causes large intensity fluctuations in the pressure drop curve as shown by fig 4.1c. The decrease in the pressure drop curve above $u_{mf}$ corresponds to the formation of channels in the bed, in which case not all the particles will be suspended thus resulting in this decline. When the channels collapse, the pressure drop rises up to the corresponding $\triangle p_{max}$ of the system and remains at this value until the next channel begins to form and this pattern continues to repeat until the channelling regime is crossed. At relatively high velocities, the bed shifts from a channeling regime to a chaotic fluidization regime, making homogeneous fluidization with 100% intermediate rods a challenge to achieve. These observations are consistent with the findings of Vollmari et al[7], who also investigated elongated particles by studying the pressure drop in the bed. In order to avoid this problem, a mixture of 90% 4.5 aspect ratio rods and 10% spheres is chosen and the pressure drop experiments are repeated. The result of these experiments are shown in fig 4.1d, from which it is clearly seen that the addition of spheres has controlled the fluctuations in the pressure drop curve, thus making

it possible to achieve a certain extent of homogeneous fluidization. Although some channeling behavior still remains, the channeling regime has become considerably smaller. Thus further experimentation with these species is done using the above specified mixture of particles. Yet another feature, noticed in this case, is the hysteresis in the pressure drop curve. Unlike in the case of spheres, when the velocity is lowered from a point larger than $u_{mf}$, the pressure curve does not follow its previous path. Thus resulting in the determination of a second $u_{mf}$. The $u_{mf}$ estimated by fluidizing a stationary bed is found to be always larger than the $u_{mf}$ estimated when the reverse is done. This phenomena can be explained as a result of pronounced entanglement of these particles, which in turn is caused by them having an aspect ratio as high as of 4.5. Consequently, they require more velocity to disentangle and fluidize them. On the contrary, when the velocity is decreased from a relatively high value, then the system is already fully suspended and can remain fluidized at a velocity lower that the previously estimated $u_{mf}$ value. For the purpose of this study, the larger $u_{mf}$ is considered as the minimum fluidization velocity of the system.

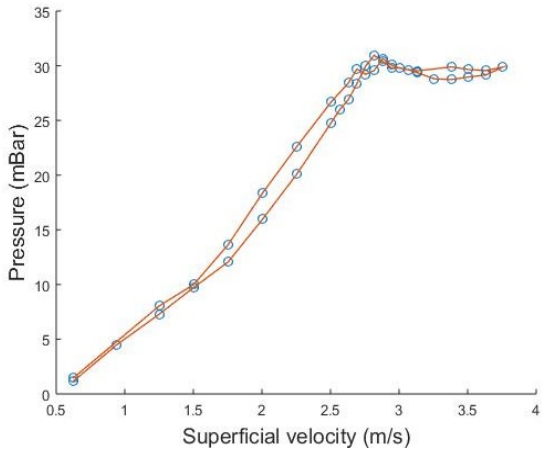


(a) Pressure drop of spherical particles (AR=1)

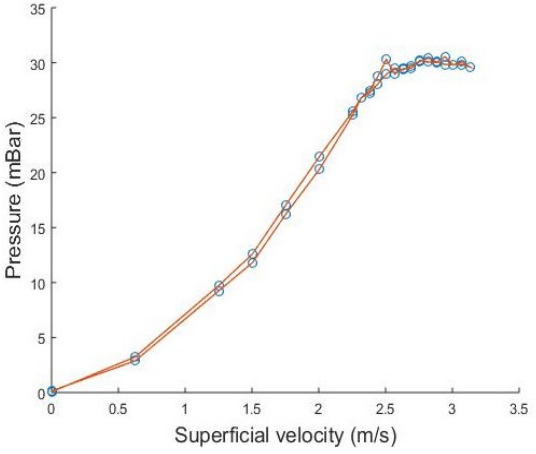


(b) Pressure drop of small rods (AR=2.25)

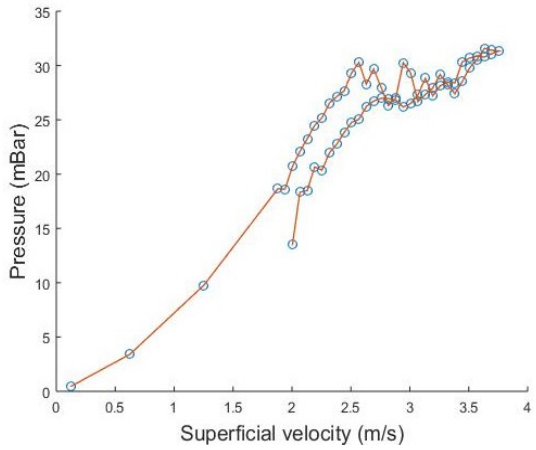


(c) Pressure drop of pure intermediate rods (AR=4.5)

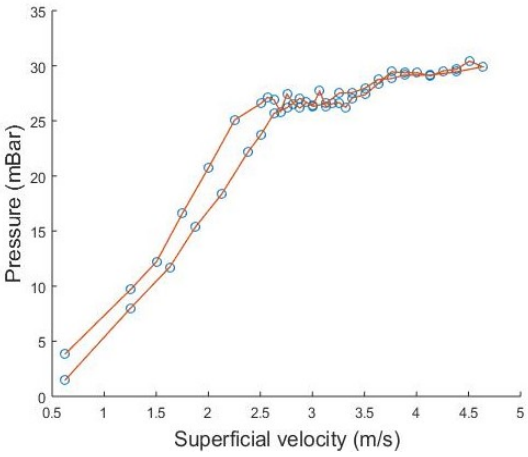


(d) Pressure drop of intermediate rod mixture (AR=4.5)

Figure 4.1: Pressure drop studies

From fig 4.1b, it is seen that the small rods (AR=2.25) behave quite similarly to that of the spheres. A small hysteresis in the pressure drop curve is noticed, leading to the estimation of two minimum fluidization velocities. However, owing to their smaller aspects ratio of 2.25, the entanglement between these particles is quite small thus the two $u_{mf}$ estimated are fairly similar.

From the pressure drop studies, it is seen that as the aspect ratio of the particle increases the minimum fluidization velocity decreases. Similar observations were made by Liu et al[29]. Table 4.1 lists the values of minimum fluidization velocities estimated for the different aspect ratio particles.

| **Particle** | **Aspect Ratio** | $u_{mf,up}$ | $u_{mf,down}$ | $u_{mf,up}/u_{mf,down}$ |
|---|---|---|---|---|
| Sphere | 1 | 2.808 | 2.804 | 1.001 |
| Small Rods | 2.25 | 2.461 | 2.492 | 0.987 |
| Intermediate Rods | 4.5 | 2.33 | 2.39 | 0.97 |
| 90% Intermediate Rod + 10% sphere | | 2.51 | 2.58 | 0.97 |

Table 4.1: Minimum fluidization velocities of the various aspect ratio particles

## 4.2 MPT Experiments

Once the fluidizing range of the different particle systems are determined from the pressure studies, the Magnetic Particle tracking experiments are conducted. Using this technique, the following properties of the particle system can be analysed:

1. Occupancy in the bed
2. Particle orientation
3. Angular Distribution
4. Translational Velocity
5. Rotational Velocity

A well know problem, when dealing with fluidized beds, is the maldistribution or the preferential flow of the fluid within the column. This could be induced as a result of several parameters such as a faulty distributor plate, a leak in the system or when the inlet fluid has a predefined flow pattern to it, and so on. When such a preferential flow occurs within a column, it is seen that there are more bubbles formed at one side of the column, meaning it causes a heterogeneity in the solid circulation pattern, i.e. some parts of the bed remain static while the other parts are well mixed. Thus it is vital to ensure that the fluidized bed has a homogeneously distributed flow inside the system.

This was also a challenge that had to be overcome with the present system, where several distributor plates were varied, the structure of the distributing chamber was altered and the chamber was filled with particles before a homogeneously distributed flow pattern could be achieved.

In order to verify that the system is homogeneously fluidized, the domain of interest is divided into a square grid with a fixed number of cells in the x, y and z directions. Each cell is a cube of size 0.01 m. The data is sorted into these cells based on the x, y and z position of the particle, thus resulting in a 3-dimensional matrix. The occupancy of each cell was estimated using Eq 4.1.

$$O\left(i,j,k\right) = \frac{N_{gridcells}}{N_{meas}} \sum_{1}^{N_{meas}} \delta\forall \begin{cases} \delta = 1 \forall p \in (i,j,k) \\ \delta = 0 \forall p \notin (i,j,k) \end{cases} \tag{4.1}$$

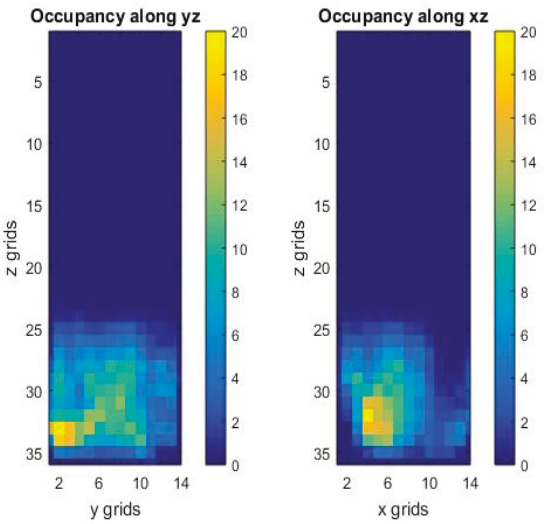


(a) Occupancy plot of a system with preferential flow

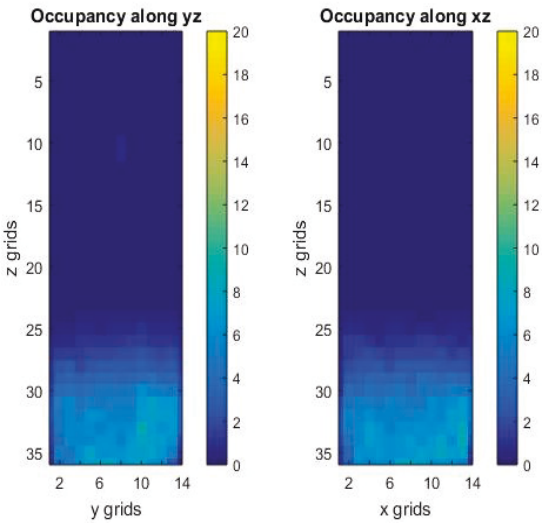


(b) Occupancy plot of a Homogeneously fluidized system

Figure 4.2: Check for Preferential Flow

A plot of the occupancy along the vertical cross section of the system, i.e. along xz and yz directions are made to see if there is preferential flow to one side of the fluidized bed. Fig 4.2a is an example of a system having preferential flow and fig 4.2b shows a homogeneously fluidized system. The yellow regions seen in fig 4.2a indicate that those cells have the highest occupancy, while the dark blue regions show that there are no particles there. Thus it is apparent that the tracer particle, in a system with preferential flow, prefers one side of the column more than the other, whereas in fig 4.2b, the occupancy of the tracer is seen to be more equally spread throughout the x and y directions of the bed, confirming the homogeneity of the system.

### 4.2.1 Strengths of MPT

In order to fully appreciate the strength of the MPT technique, the case of 4.5 aspect ratio rods fluidizing with an excess gas velocity of 1.5m/s is explained in detail. The bed aspect ratio for this scenario is taken to be 0.75, i.e. $H_{bed}/D_{bed} = 0.75$.

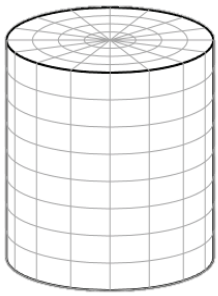

(a) Cylindrical grid

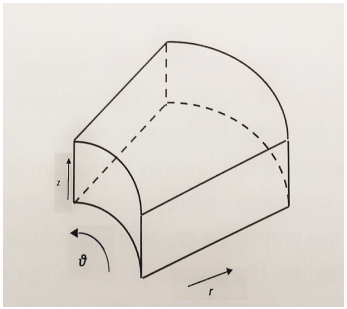

(b) Representation of a single cell in the cylindrical grid

Figure 4.3: Cylindrical Representation

### Cylindrical Occupancy

Once homogeneous flow is established the domain of interest is divided into cylindrical grids as shown in fig 4.3a. This is done taking the geometry of the system into consideration and to differentiate between wall and bulk behavior of the particles. The grid specifications have been mentioned in Table 4.2. The representation of a single cell is shown in fig 4.3b. The cell interfaces in the r-$\theta$ plane and the r-z plane have toroidal and rectangular shapes respectively.

| **Property** | **Direction** | | |
|---|---|---|---|
| | **r** | $\theta_c$ | **z** |
| Actual domain | 0.087 (m) | $2\pi$ (rad) | 0.46 (m) |
| Grid size | 0.01 (m) | $2\pi/36$ (rad) | 0.01 (m) |
| Number of grids | 7 | 36 | 46 |

Table 4.2: Grid specification

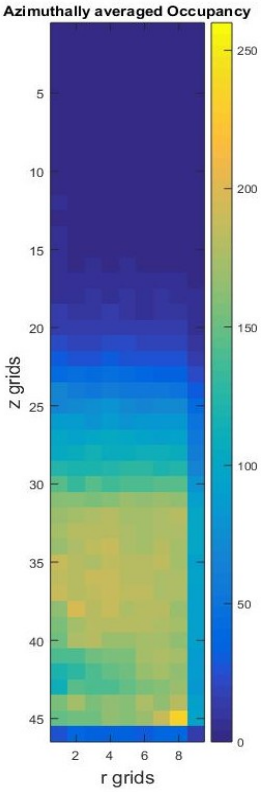


Figure 4.4: Azimuthally averaged occupancy plot

The recreated path of the tracer is then sorted into these grids cells for further analysis. The occupancy of each cell is estimated as before. As the system has similar behavior azimuthally, an azimuthally averaged occupancy plot, shown in fig 4.4, is made to see the occupancy along the radial and z directions. Thus providing information on the extent of bed expansion and local bed density. The occupancy of these cells are corrected for the effect of $r^2$. From the figure it is observed that there is a sudden decrease in bed density near the wall, this is a result of the particle's cylindrical geometry, by the virtue of which it tends to pack more tightly in the bulk of the bed, i.e. the particles can pack more tightly when packed amongst themselves than when packed against a flat surface.

**Translational Velocity**

From MPT, the x,y and z positions of the tracer particle is obtained as a function of time. Using the particle positions, the velocity of the particle in x-direction is computed by Eq 4.2, where dt is calculated with the sampling frequency. The y and z velocities are determined in a similar fashion. The velocity of the particles in the radial direction are then estimated using Eq 4.3, where $\theta_c$ is the azimuthal angle estimated for the cylindrical column according to Eq 4.4. A plot of the radial velocity versus the z-velocity is considered. Fig 4.5 shows the azimuthally averaged velocity profile of 4.5 aspect ratio rod mixture at an excess gas velocity of 1.5m/s, where the colours represent the intensity of the linear velocities in a particular region in the bed and the directionality of the arrows provide the direction of solid flow. The figure shows an upflow of the solids near the wall region closer to the distributor plate while higher up in the bed, this upflow region moves slightly away from the wall and downflow velocities are noticed at the central regions and close to the walls. Such flow patterns have been reported in Kuni&Levenspiel[12] for Geldart B particles, whose bed aspect ratio also approaches unity. Thus the figure gives a good qualitative description of the solid circulation in the bed.

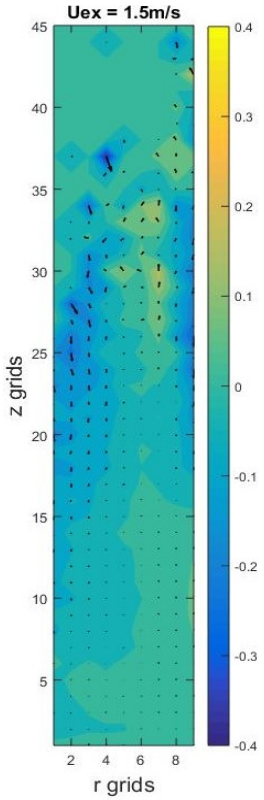


Figure 4.5: Linear velocity profile at a excess velocity of 1.5m/s

$$U_x = \frac{x_{t+1} - x_t}{dt} \tag{4.2}$$

$$U_r = U_x * \cos(\theta_c) + U_y * \sin(\theta_c) \tag{4.3}$$

$$\theta_c = \arctan(y, x) * \frac{180}{\pi} \tag{4.4}$$

### Rotational velocity

One of the biggest advantages of the MPT technique is its ability to capture the orientation of the particle as a function of time. Eq 4.5 is used to estimate the rotational velocity of the tracer, where $\overline{e}_t$ is the orientational unit vector of the particle at time t. The rotational velocity is estimated in rot/s. Fig 4.6a shows an azimuthally averaged rotational velocity profile of the particle in the bed. In the case of these elongated rods, it seen that, at the base of the column, there is no gradient in the rotational velocity along the radial direction, however near the top of the bed a strong radial gradient is seen. In order to clearly observe this profile, the bed is divided into 3 equal regions along the height, and a height averaged rotational velocity is plotted as a function of the radial grid cells, shown in fig 4.6b. Comparing these profiles with the linear velocity profiles shown in fig 4.5, it can be seen that the rotational velocity is at its highest in a region where the upflowing solids change their direction of flow. This shows that the granular circulation pattern of the particle plays an influencing role in its rotational behavior. Moreover at the higher bed heights, the porosity of the bed is quite large enabling the particles to rotate freely and unhindered by the effects of particle-particle entanglement.

$$\omega_p = \frac{\arccos\left(\overline{e}_t \cdot \overline{e}_{t+\triangle t}\right)}{2\pi \triangle t} \tag{4.5}$$

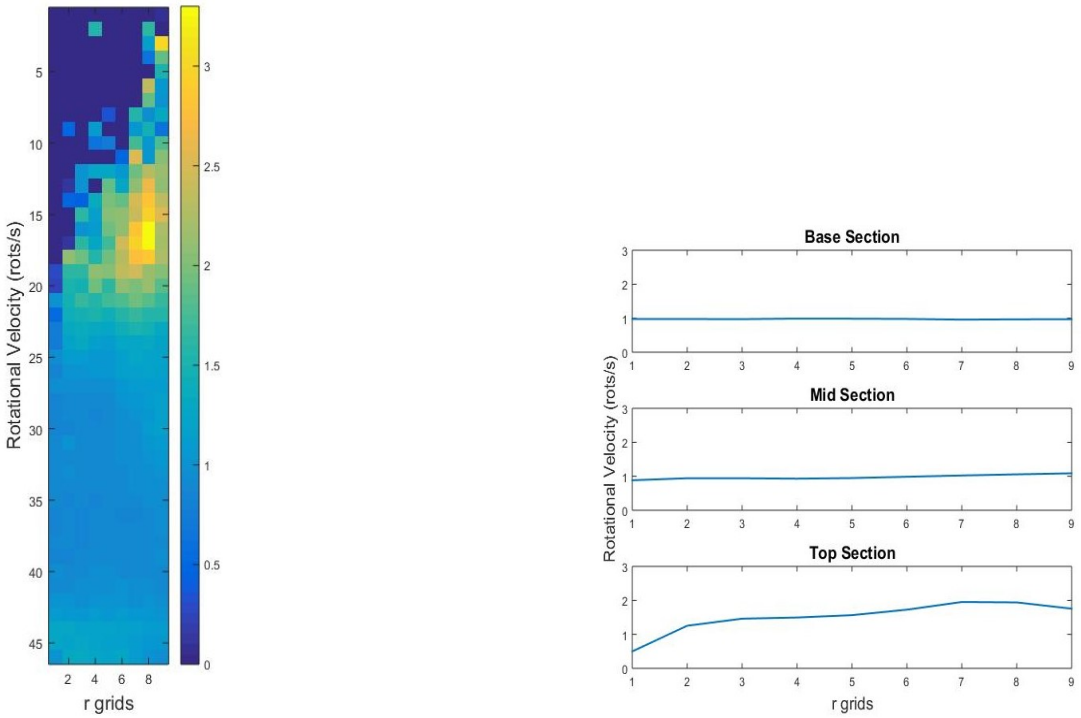


(a) Azimuthally averaged rotational velocity

(b) Averaged rotational velocities at different bed heights

Figure 4.6: Rotational velocities at excess gas velocity of 1.5m/s

It is essential to realize that in this study, the spin of the particle is not accounted for, i.e. the full magnitude of the angular velocity is not captured but rather only the angular velocities that is defined by the axes perpendicular to the magnetic axis of the particle is accounted for.

### Angular Distribution

In order to realize the effect of the Helmholtz coil and to make sure the magnetic tracer is completely unbiased by the earth's magnetic field, a test of fluidization, with and without the

Helmholtz coil is done and its results are shown in Appendix A.3. Once this is ensured, the angle of inclination '$\theta$' and the azimuthal angle '$\varphi$' can be analysed further. Fig 4.7 shows the representation of the angle of inclination and azimuthal angle for an elongated particle.

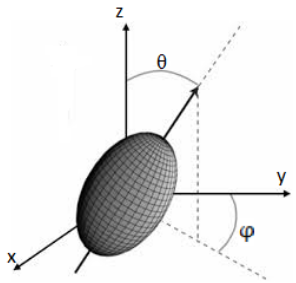


Figure 4.7: Representation of $\theta$ and $\varphi$

**Angle of inclination '$\theta$':**

The angle of inclination is computed using the Eq 4.6, where $e_x$, $e_y$ and $e_z$ are the orientational unit vectors in the x, y and z directions respectively. The range of $\theta$ provided by this equation is [0 180].

$$\theta = acos\left(\frac{e_z}{\sqrt{e_x^2 + e_y^2 + e_z^2}}\right) * \frac{180}{\pi} \tag{4.6}$$

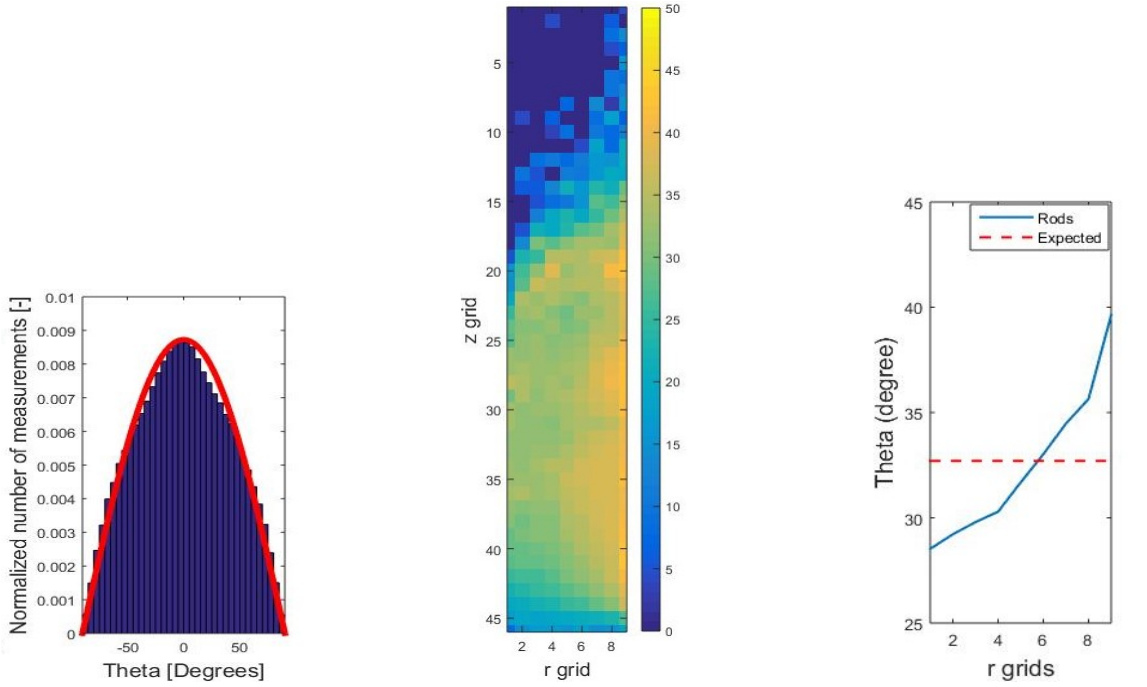


(a) Distribution of $\theta$ in the bed (b) Profile of $\theta$ in bed (c) Height average profile of $\theta$

Figure 4.8: Behavior of $\theta$ at excess velocity of 1.5m/s

The angles 0° and 180° represent vertical orientation of the particle, i.e. particle aligned along the flow in bed. Since, there is no significant difference in the orientations represented by the angles 0° and 180° for this study, the range of $\theta$ is taken between [-90 90] and the absolutes of

these values are then taken into consideration for further analysis. Thus, 90° will now represent the vertical orientation of the particle and 0° will correspond to a horizontally aligned particle. The distribution of the angles in the bed is shown, for the entire range of $\theta$, in fig 4.8a and it is seen that the distribution on either side 0° is a mirror image of the other. Thus confirming that there is no preference between the orientations represented by 90° and -90°. A slight deviation from the expected behavior, represented by the red line, is observed.

The cause of this deviation is investigated by viewing the azimuthally averaged profile of $\theta$ in the bed, shown in fig 4.8b. Looking at the height averaged profile of $\theta$, in fig 4.8c, it is seen that the angle of inclination is a function of particle's radial position and deviates from the expected. This profile indicates that rods have a higher preference to align horizontally at the central regions of the bed, while they are found to be more vertically oriented near the outer regions. A sharp increase in $\theta$ at the wall confirms that the presence of walls, forces the particles to align along the walls.

**Azimuthal angle '$\varphi$':**

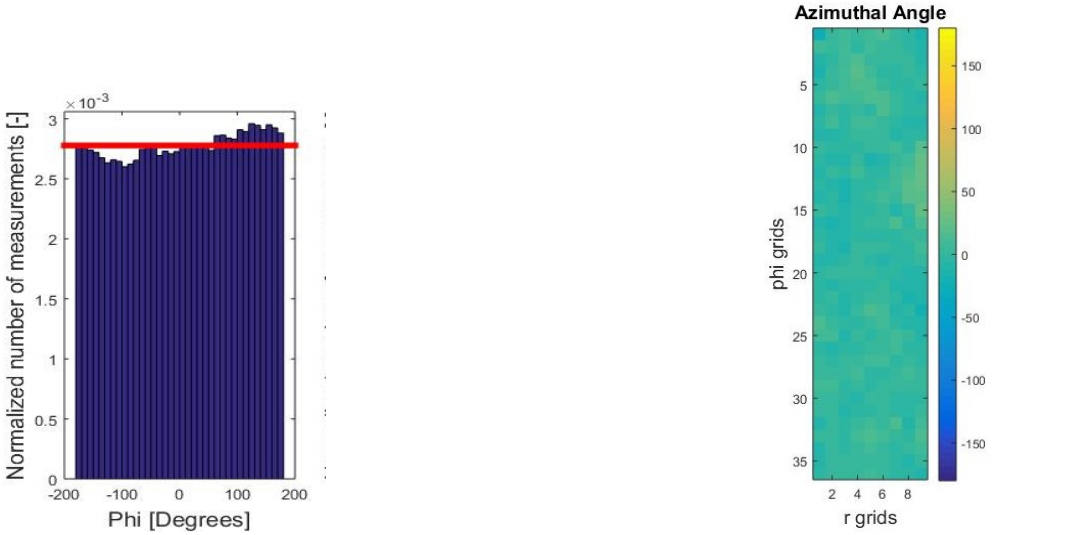


(a) Distribution of $\varphi$ in the bed

(b) Height average behavior of $\varphi$

Figure 4.9: Behavior of $\varphi$ at excess velocity of 1.5m/s

The azimuthal angle of the particle $\varphi$ is computed as shown by eq 4.7 and the range of $\varphi$ obtained is [-180 180]. The distribution of azimuthal angle is shown by fig 4.9a. When a profile of $\varphi$ is viewed as a function of r and $\theta_c$, shown in fig 4.9b, it is seen that there are no gradients either along the r or along $\theta_c$. No specific wall effects are noticed in this case and it can be concluded that the azimuthal orientation of the particles seem uninfluenced by the presence of the wall. It was also confirmed that, no gradient was observed along the height of the column.

$$\varphi = \arctan(e_y, e_x) * \frac{180}{\pi} \tag{4.7}$$

### 4.2.2 Effect of superficial velocity

Now that the capabilities of the MPT technique are clear, a deeper analysis of the behavior of the different aspect ratio particle system is conducted. This can be done by examining the different aspect ratio systems under varying excess gas velocities from 0.5m/s to 2.5m/s and for a bed aspect ratio 0.75, i.e. $H_{bed}/D_{bed} = 0.75$. Figures 4.10 and 4.11 show the various properties of the spheres and 4.5 aspect ratio rod mixtures, for various excess gas velocities.

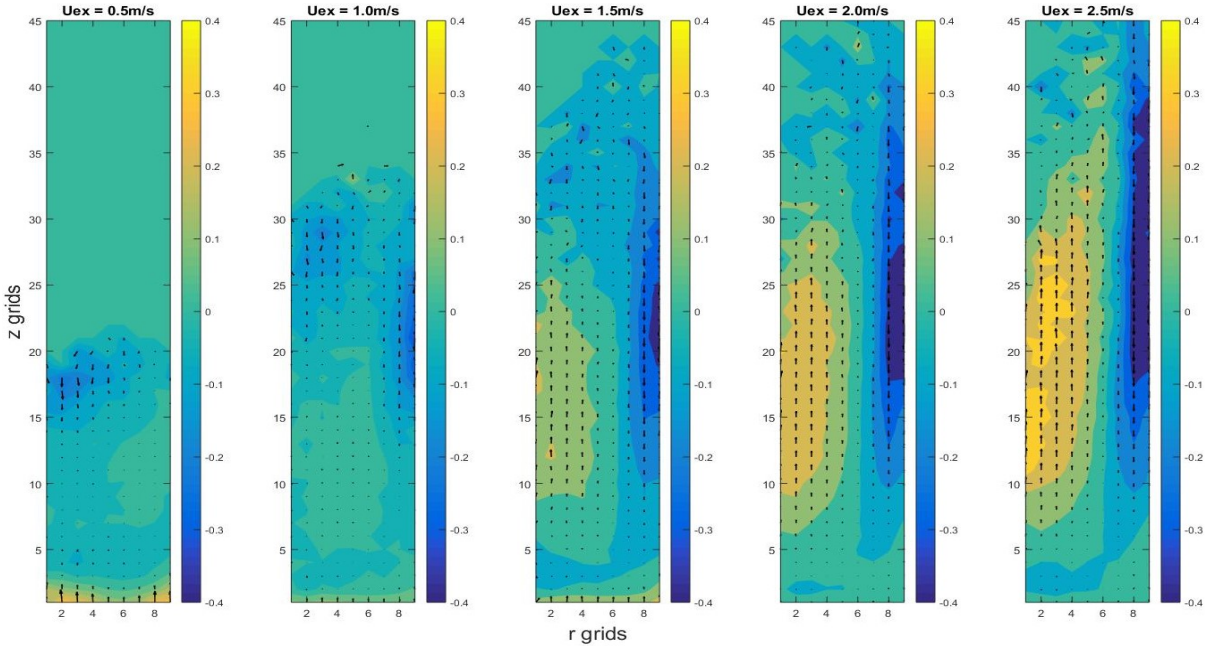


(a) Linear velocity profiles

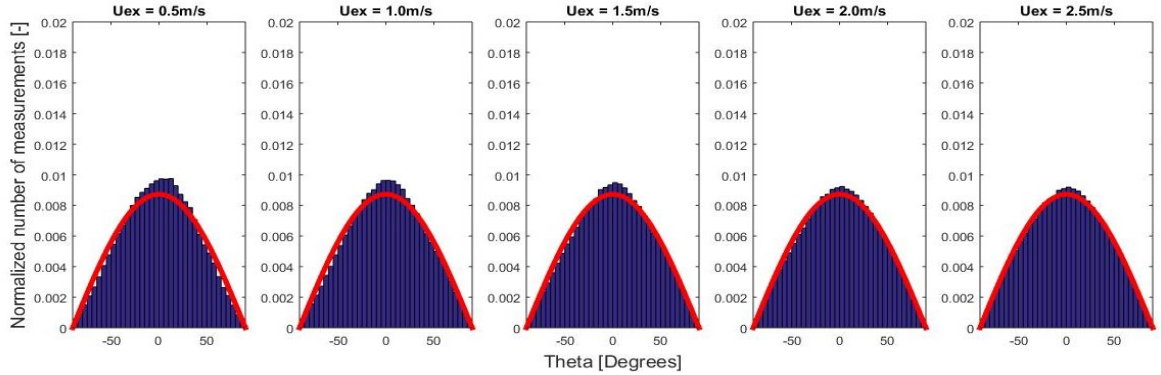


(b) Distribution of $\theta$

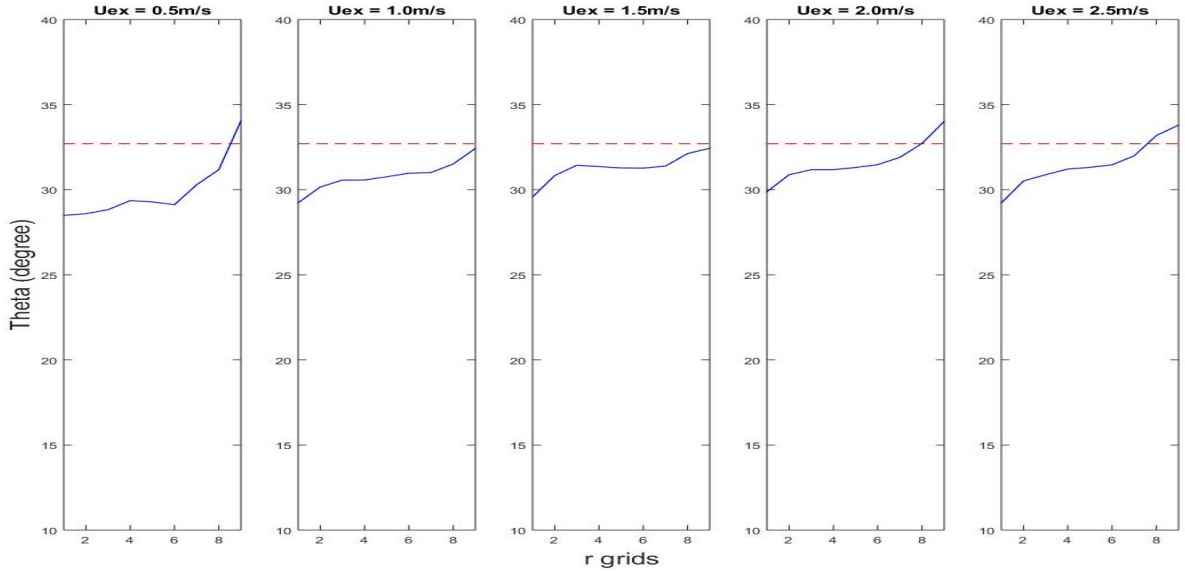


(c) Average $\theta$ along the redial direction

Figure 4.10: Behavior of spherical particles (aspect ratio=1) for various excess gas velocities

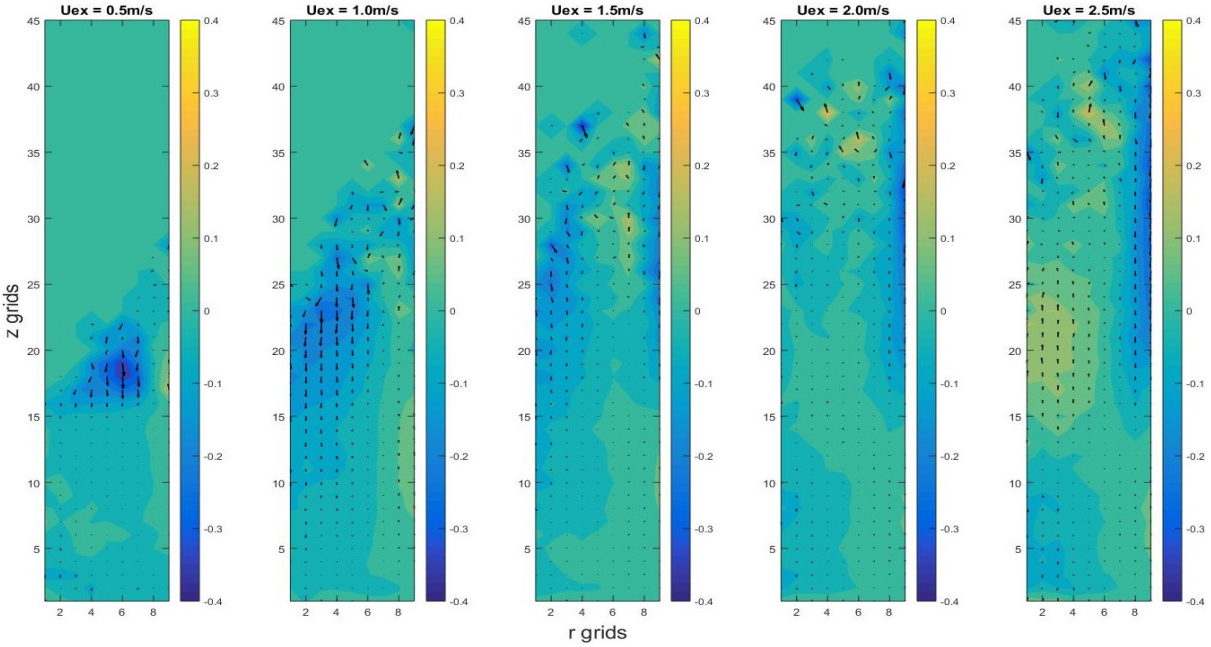


(a) Linear velocity profiles

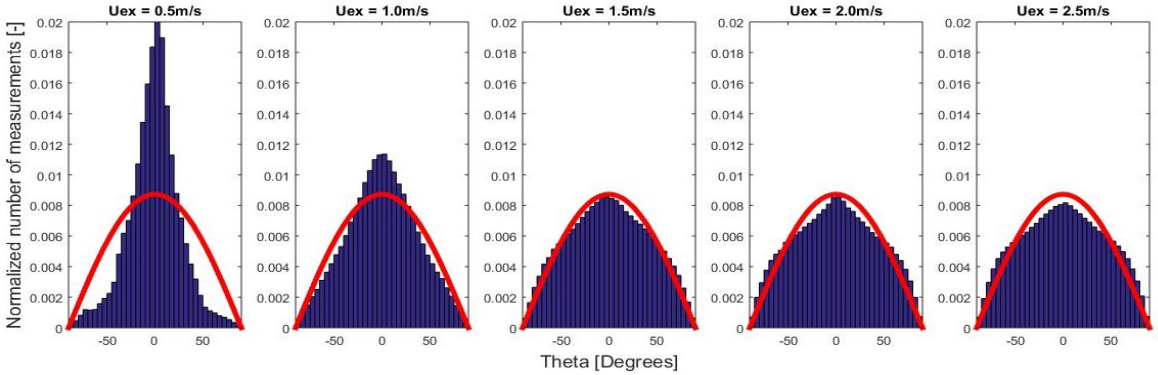


(b) Distribution of $\theta$

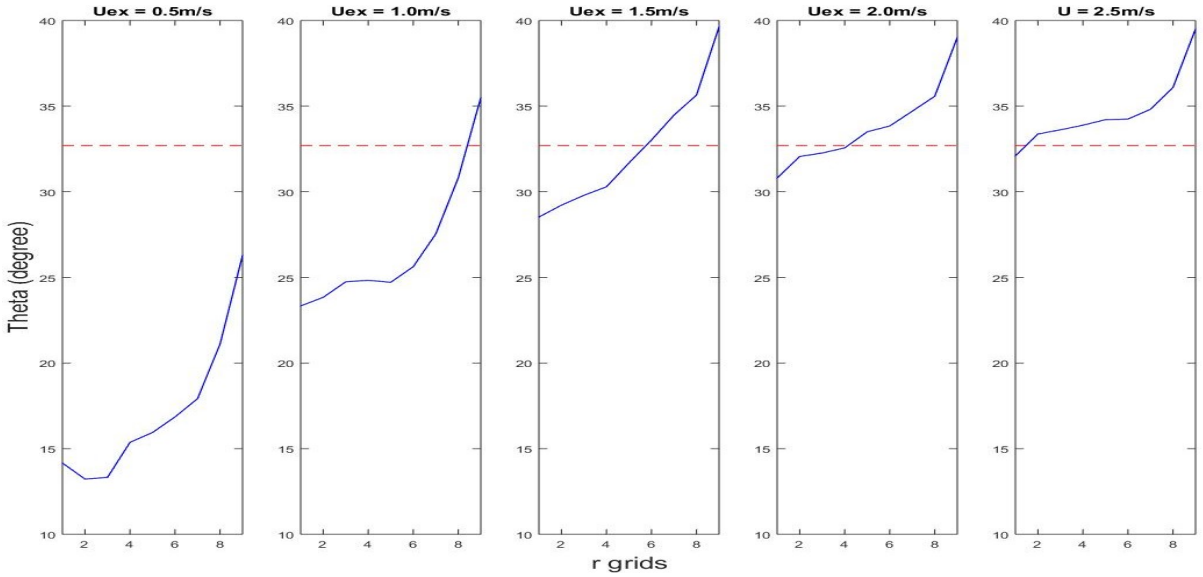


(c) Average $\theta$ along the redial direction

Figure 4.11: Behavior of 4.5 aspect ratio rod mixture for various excess gas velocities

From fig 4.10a it is seen that, for low gas velocities the spheres circulate with an upflow at the wall and downflow at the central regions of the bed. However, with the increase in the superficial gas velocity, the direction of granular circulation reverses to have upflow at the central regions of the bed and downflow at the walls. Such reversal of granular circulation pattern was reported in the Kuni & Levenspiel[12], for Geldart B particles for a bed aspect ratio less than unity. The reason cited for this behavior, is the large rising of bubbles in the bed. With the increase in superficial gas velocity, the bed shifts from a *bubbling fluidization regime* to a *churning fluidization regime*, where large scale uniform motion and gross circulation of the bed material is seen.

Fig 4.11a shows the Linear velocity profiles for the 4.5 aspect ratio rod mixture, for the same excess gas velocities. It can be seen that, in this case too, the reversal in circulating pattern is present however this reversing takes place at a much higher gas velocity than in the case of spheres. It is also seen that this transition is more gradual in rods than it is in the case of spheres. This maybe because the large rising of the bubbles in the bed is hindered by the enhanced particle entanglement present in the rods. This also results in the rods having a lower solid velocity than the spheres, which is apparent from comparing fig 4.10a with fig 4.11a. Zitoun et al[5] also noticed that the motion of elongated particles is restricted by its interaction with solids phase. Furthermore, It is observed that the fluidization of the rods at high flowrates resembles the fluidization of particles in a deep bed, even though the aspect ratio of the current bed is less than unity.

Varying the superficial gas velocity not only affects the granular circulation patterns but also has an influence on the orientation (inclination) of the particles in the bed. This is clearly seen from fig 4.11b and 4.11c that show the distribution of $\theta$ in the bed and the average $\theta$ along the radial direction respectively, for the case of rods. Looking at the distribution of $\theta$ in the bed, it is apparent that at lower gas velocities the rods have a strong preference to be inclined at 0°, i.e. they tend to be horizontal and align themselves perpendicular to the flow. However with the increase in gas velocity it is seen that this preference gradually changes and the distribution of $\theta$ in the bed tends to become flatter with the rising gas velocity. This implies that at higher gas flowrates, more rods are aligned along the flow and the amount of horizontally oriented rods decrease. This result is in accordance with Vollmari et al[7] findings in a square fluidizing column and of Ku and Lin's[30], who examined the orientation of cylinders in a pipe flow with direct numerical simulation using the Lattice Boltzmann method. The sharp peak seen for the distribution at $u_{excess}$ 0.5m/s is a result of severe channelling of the system, implying that a major portion of the bed is static except at the channels. It is visually observed that at channeling regime,the static particles are horizontally placed while the particles in that channel are oriented along the flow but these channels fluidize only a small fraction of the entire bed and thus resulting in the sharp distribution. The average $\theta$ along the radial direction, fig 4.11c, confirms that the inclination of the rods is not only a function of the gas velocity but also depends on the particle's radial position in the bed. The orientation of the particles, in the vicinity of the walls, are more vertical than the bulk, for all gas velocities suggesting that the presence of wall is always felt by an elongated particle.

Because of their shape, the angle of inclination $\theta$ in a sphere, is expected to have no specific preference and to be independed on both the gas velocity and its radial position in the column. This is indeed true and can be confirmed from the fig 4.10b where it can be seen that the expected behavior represented by the red line is always adhered to and from fig 4.10c where is apparent that there is no radial preference.

The rotational behavior of the spheres and rods is yet another intersing property to investigate. Fig 4.12 shows the rotational behavior of the spheres and 4.5 aspect ratio rods as a

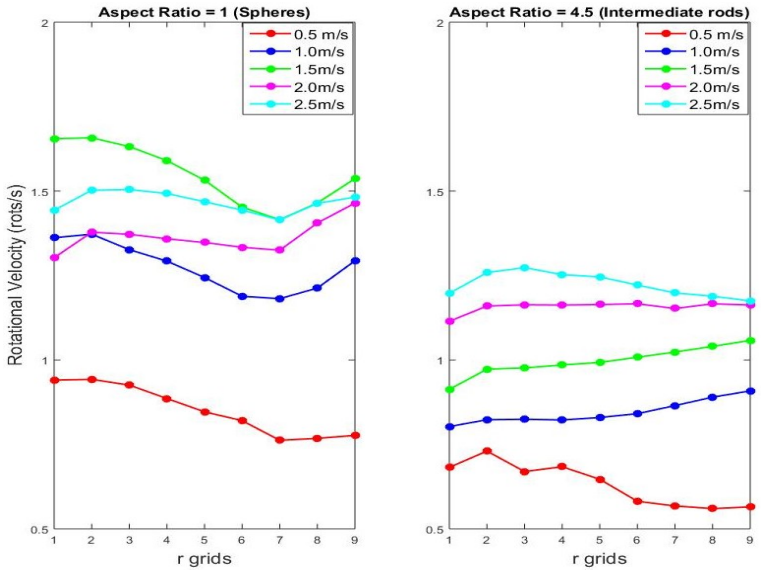


Figure 4.12: Rotational velocity along the radial direction for various excess gas velocities

function of their radial position for various excess gas velocities. From the figure it is apparent that the spheres have a distinct rotational profile radially. It can be seen that the rotational velocity of the sphere is higher in regions where the linear velocities are dominant, suggesting that in those regions the shear force felt by the spherical particles are higher consequently, causing it to rotate faster. However, this trend is not seen in the case of 4.5 aspect ratio rods. They seem to have a flat profile radially and have lower magnitude of rotational velocity than spheres. This is caused by the high aspect ratio of the rods, by the virtue of which they tend to align themselves according to the flow and thereby reducing their freedom of rotation. Additionally the dense bed offers a limited free space and induces more collisions with the walls and other particles thus further resisting the rotation of the rods. This was confirmed by looking at the rotational velocities of the spheres and rods at different bed heights, which showed that spheres had higher rotational velocities at the base of the column while the rods had large rotational velocities only at the top of the column.

Having seen that the shear force influences the rotations in a sphere, it becomes intriguing to see the influence of the inlet gas velocity on the particle's rotation. The increase in the gas flowrate is expected to create an imbalanced in the pressure equilibrium around the particle, which tends to increase their rotations. This is verified by plotting the mean rotational velocity in the bed as a function of its excess gas velocity. Fig 4.13a shows that there is a slight increase in the rotational velocity of spheres until $u_{excess}$ 1.5m/s and then a slight dip in the profile. This decrease maybe caused by the shift from bubbling to churning fluidizing regime of the bed. Rods also show an increase in rotational velocity with the increase in inlet gas velocity, but the magnitude of increase remains lower than spheres.

In order to realize the effect of walls on the rotational behavior of the particles, fig 4.13b which shows the rotational velocity of the particle present in the vicinity of the wall, is made. From the figure it is clear that for these particles, the rotational velocity at the wall is almost the same as its mean rotational velocity.

To check if the occupancy of the particles in the bed is a function of gas velocity, the occupancy profile of the bed for various gas velocitites are compared for spheres and rods. Such a comparison indicated that the expansion of the bed, for a specific gas velocity, is higher in case of spheres. To investigate this further and to check if the occupancy in the bed has a radial

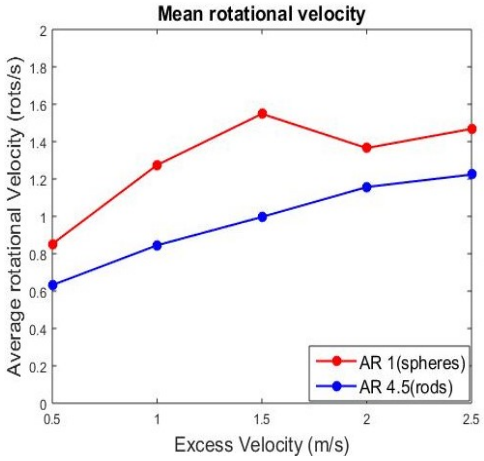


(a) Mean rotational velocity as a function of excess gas velocity

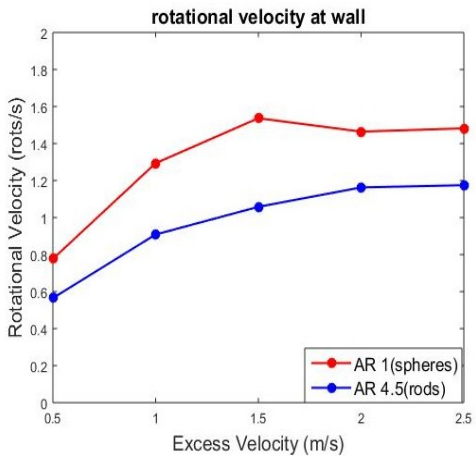


(b) Rotational velocity at wall as a function of excess gas velocity

Figure 4.13: Rotational Velocity behavior of spheres and 4.5 aspect ratio rods

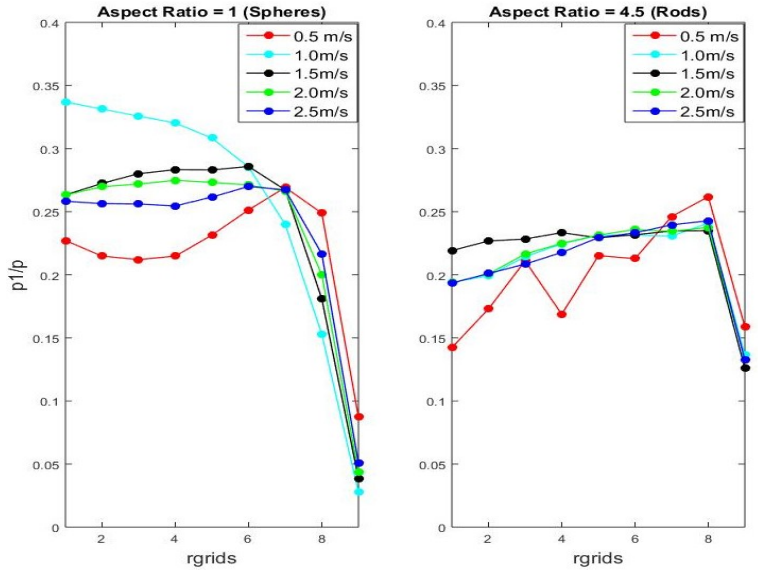


Figure 4.14: Virtual particle concentration

profile, a kind of virtual particle concentration is estimated, based on the Monte Carlo computational algorithm, where the frequency of finding the particle in a specific region is computed. A detailed explanation on this approach is given by Zhang et al[16]. Fig 4.14 shows virtual particle concentration as a function of radial position for varying gas velocities and for both the spheres and 4.5 aspect ratio rods. Here 'p1' is the frequency of occurrence of particle in a certain radial region and 'p' is the total frequency of occurrence of the particle in the bed, i.e. first the position of the tracer particle is recorded for the entire time of fluidization and then count the number of times the tracer is found in a certain region, this is taken as p1 and the total number of instances recorded is taken as p. Thus p1/p gives a virtual concentration of the particles in the bed. This virtual concentration is corrected for the effect of $\triangle r^2$. The figure indicates that the occupancy, along the radial direction is not affected much by the inlet gas velocity for both the spheres and rods. The main observation here relates to the wall effect, which causes a sudden increase in the bed porosity in its vicinity. It is seen that this effect is more prominent in a sphere of equivalent volume, owing to its larger radius.

### 4.2.3 Effect of Bed Height

To see if the bed height, i.e. the amount of particles in the system, has an effect on its behavior, two aspect ratios of the bed ($H_{bed}/D_{bed} = 0.5$ and $H_{bed}/D_{bed} = 0.75$)are examined and those results are discussed in this section. For this discussion, consider the behavior of the spheres and 4.5 aspect ratio rods for an excess gas velocity of 1.5m/s. For efficient comparison of the linear velocities, a height averaged velocity is considered and it is plotted as a function of the radial position. Fig 4.15a shows the averaged linear velocity profiles of the both the spheres and 4.5 aspect ratio rods for the different bed heights and it is apparent that the velocity gradient along the radial direction is slightly more prominent when the amount of material in the system is higher. However the shape of the profiles are maintained for both the rods and spheres. Examining the system of 4.5 aspect ratio rods with a lower bed height ($H_{bed}/D_{bed} = 0.5$) revealed that the reversal in granular flow direction does not occur for the given range of excess gas velocities. At $u_{excess}$ 2.5m/s the system is still in the transitional regime indicating that the flow reversal might occur at a larger inlet gas velocity. This phenomena is not seen for sphere, as the flow reversal occurs in the same gas velocity for both the bed heights. Another observation is that a higher concentration of the rod like particles aid in the aligning the rods along the flow. This can be confirmed by looking at scenario for the rods in fig 4.16, where it can be seen that the distribution of $\theta$ for the smaller bed height shows a higher preference for the horizontal alignment of the particles while the distribution for the larger bed height at the same excess gas velocity, has already begun to flatten out, suggesting that more rods are aligned vertically than in the former scenario.

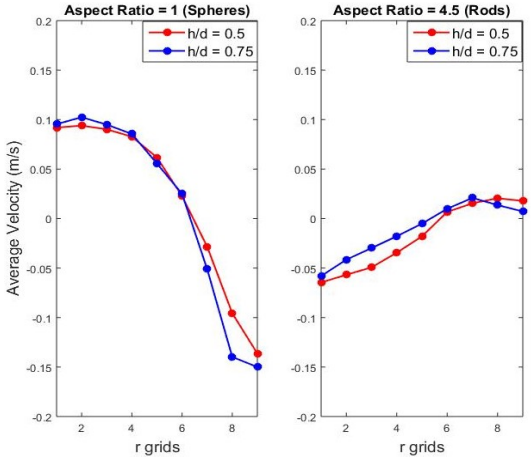


(a) Height averaged linear velocity profile along the radial direction

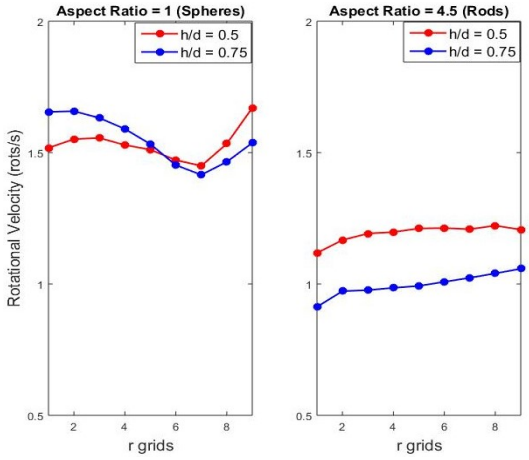


(b) Rotational velocity profile along the radial direction

Figure 4.15: Velocity profile comparison at $u_{excess}$ 1.5m/s

Fig 4.15b shows the behavior of the rotational velocities for the case of spheres and rods at different bed heights. The rotational velocity of the rods decreases with the increase in number of particles in the bed. This is the expected, as the increase in particle concentration results in increased interaction between the particles and thereby decreasing the free space available for rotation. A similar effect was seen by Ku et al[30] for the case of cubic particles. However, no such prominent change in rotational behavior is seen for the spheres.

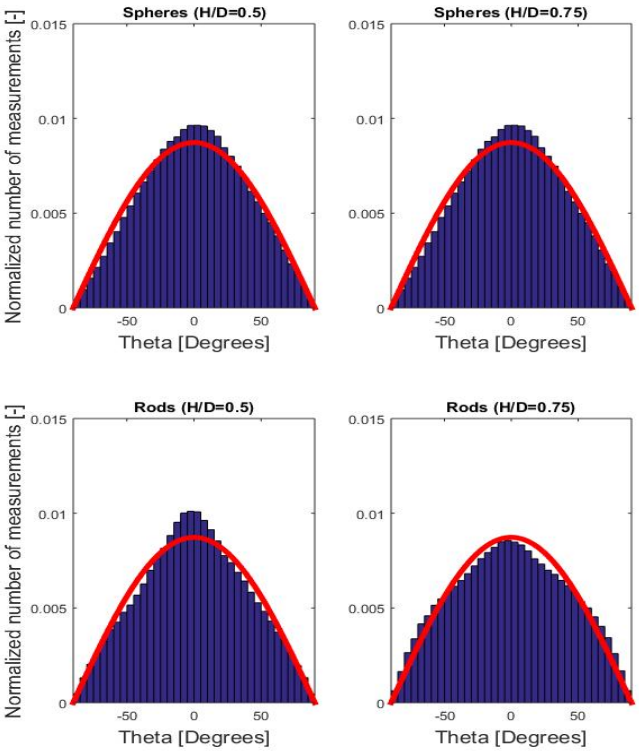


Figure 4.16: Distribution of $\theta$ at $u_{excess}$ 1.5m/s

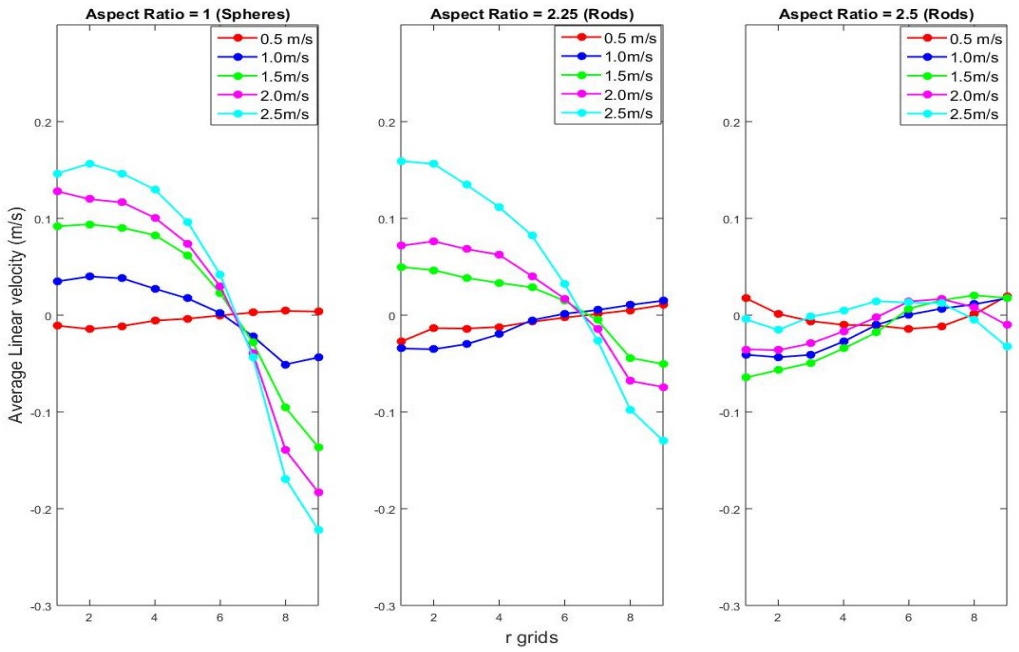


Figure 4.17: Height averaged linear velocity profile along the r for the different particles

### 4.2.4 Effect of Aspect ratio of Particle

In order to understand how the aspect ratio of the cylindrical particle affects the behaviour of fluidization, the above experiments were also repeated for the 2.5 aspect ratio cylindrical particles for a bed height of $0.5 * D_{bed}$. Fig 4.17 shows the height averaged linear velocity profiles for the different aspect ratio systems and it can be seen from the velocity profiles that the behavior of the 2.25 aspect ratio rods is quite similar to that of the sphere while there is a marked difference when compared with the 4.5 aspect ratio rods. Similar to spheres, the 2.25 aspect ratio rods also undergo the reversal of granular circulation at a low excess gas velocity and this transition is fairly sharp. The detailed velocity profiles for the 2.25 aspect ratio rods are shown in the appendix A.4. Contrastingly, the 4.5 aspect ratio rods show an almost flat profile in the radial direction that shows very small gradient change for the different gas velocities. This means that, for the given range of excess gas velocities and bed aspect ratio combination, a real circulation pattern is not yet established. This finding is in line with Cai et al's[4] and Vollmari et al's[7] results, where it is shown that particles with an aspect ratio less than 4 can essentially be treated as spheres.

Looking at the rotational velocity profiles for the different particle systems, it can be said that both the 2.25 aspect ratio rods and 4.5 aspect ratio rods, unlike spheres, have a flat rotational velocity gradient along the radial direction. Even though the rotational velocities of the 2.25 aspect ratio rods are expected to be in higher than the 4.5 rods and in par with spheres, a slightly lower rotational velocities seen for these 2.25 aspect ratio rods. This is probably because these rods where made from SS303 material which is slightly more magnetizable than the SS316. Thus rendering these particles completely unmagnetizable was not possible and as a result the rotational motion of the tracer magnet could have been hindered by the mild attraction between the tracer and the bed material.

Fig 4.19 shows the average inclination of the different particle systems, from which it is seen that, the orientational behavior of the 2.25 aspect ratio rods always lies in between the spheres and 4.5 aspect ratio rods. For lower gas velocities the 2.25 rods orient similar to the longer rods, however at increased gas flow rates their behavior is more similar to spheres.

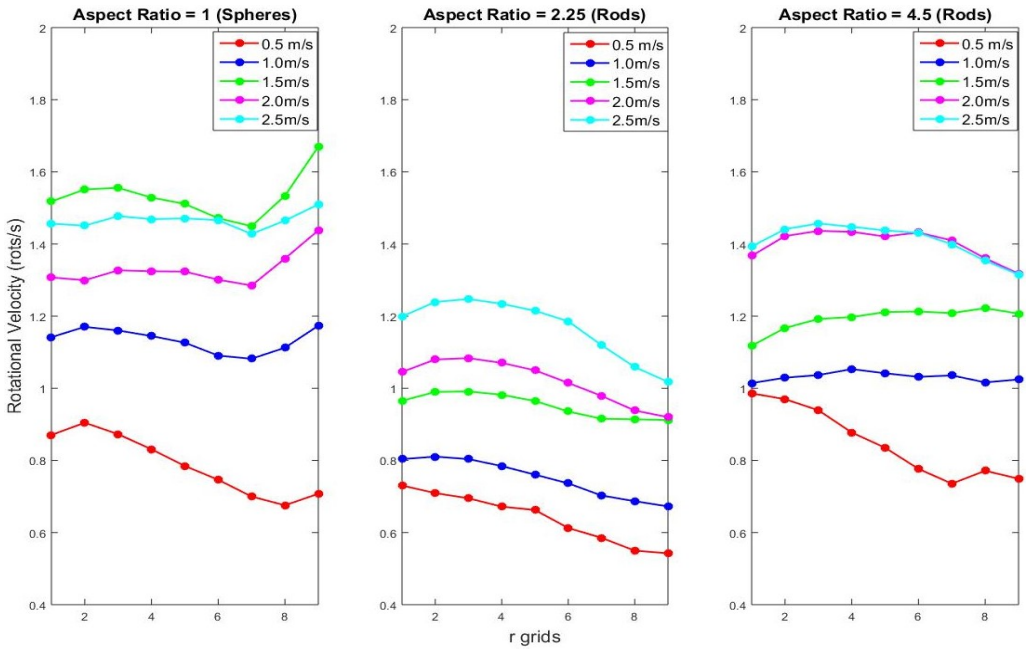


Figure 4.18: Rotational velocity profile along the r for the different particles

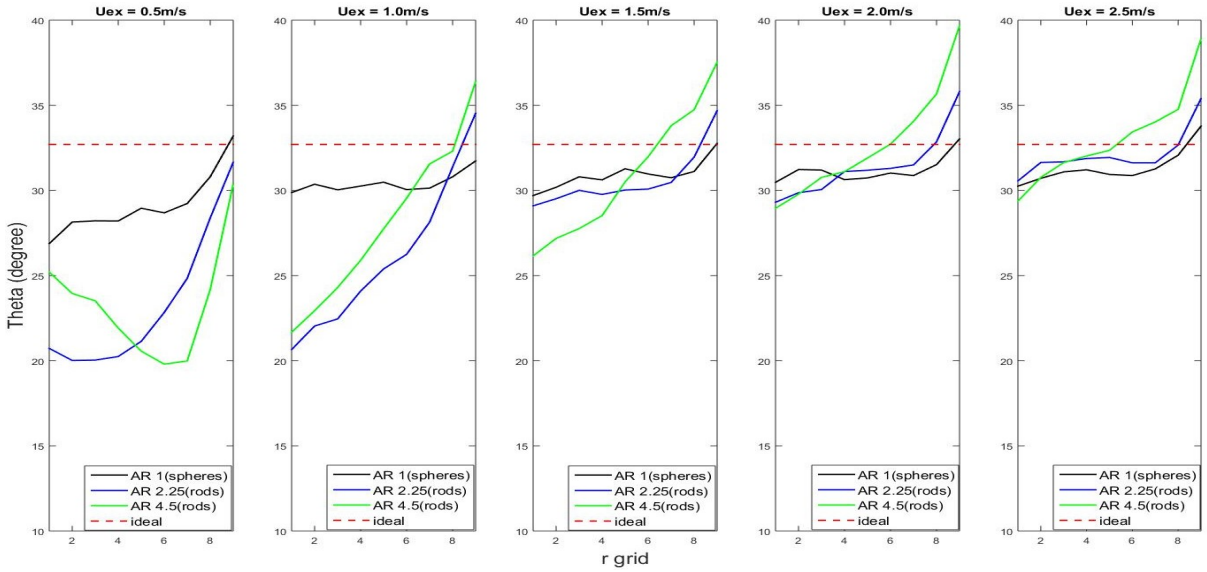


Figure 4.19: Average $\theta$ along the r for the different particles

## 4.3 TFM vs Experimental results

In order to realize the extent to which the TFM simulations are able to reproduce the experimental results, an existing Two Fluid Model, as described by Verma et al[31], was selected and the input parameters corresponding to the experimental setup was used. The simulation was run for a real time of 30 seconds in order to ensure there were statistically enough data points. The drag model selected for these simulations is the 'Ergun and Wen&Yu'. The grid sizes, number of particles and initial bed height were maintained the same as the experimental values. The time step used was $1.0 * 10^{-4}$s. In order to represent the different aspect ratio particles and see the effect of non sphericity in the simulation, the shape factor is altered to the corresponding sphericity of the particles being simulated. The time and azimuthally averaged simulation and experimental velocity profiles are first compared for the excess gas velocity of 1.5m/s for all the 3 particle types and their results are shown in fig 4.20, 4.21 and 4.22.

From the comparisons, it can be seen that for all the cases, the TFM over predicts the solid velocities in the bed and the bed expansions. Moreover it is observed that the prediction deviates more with the decreasing sphericity factor, i.e. the velocity profile prediction worsens for the higher aspect ratio particles. Fig 4.20 shows a qualitative agreement in the velocity profile for the spheres, where both the simulation and experiment shows an upward velocity at the central regions of the bed and downward velocity at the walls. However, TFM predicts a higher bed expansion than what the experiments shows. From fig4.21 a similar trend is observed wherein, the velocity profiles are a qualitative match. This is yet another confirmation, that particles with an aspect ratio smaller than 4, behave quite similar to spheres. Comparing the simulation figures 4.20a and 4.21a it can be said that the shape factor doesn't seem to play a prominent role for the velocity profiles in the bed, however its role is visible in the expansion of the bed. The 2.25 aspect ratio rods have a lower superficial gas velocity than the sphere, for the same value of excess gas velocity, yet the bed expansion predicted for the small rods are larger. This larger bed expansion of the small rods in comparison to the spheres, is also noticed in the experimental results, although the value of expansion is still over predicted by the simulation. The reason for this increase in bed expansion is that, the cylindrical particle always tries to maximize its drag in the system and consequently travel faster in a channel when compared to a sphere of its equivalent volume[2]. Thus the simulation is able to capture this aspect because the shape factor used is incorporated into the drag model that is used to describe the solid flow.

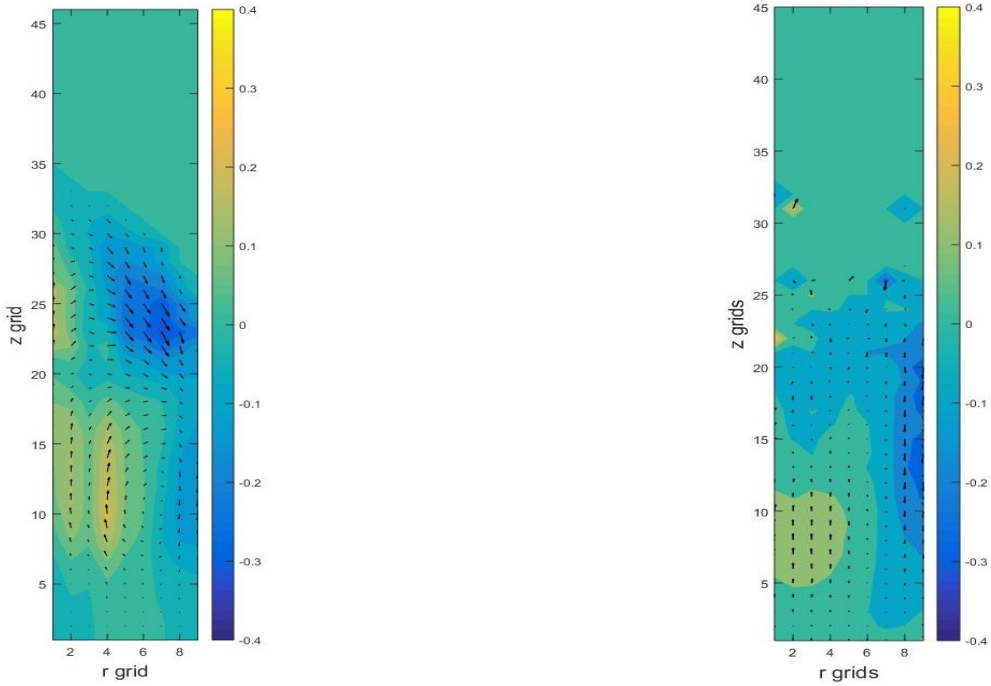


(a) Velocity profile predicted by TFM (b) Experimental velocity profile

Figure 4.20: Velocity profiles of Spheres (aspect ratio=1) for excess velocity of 1.5m/s

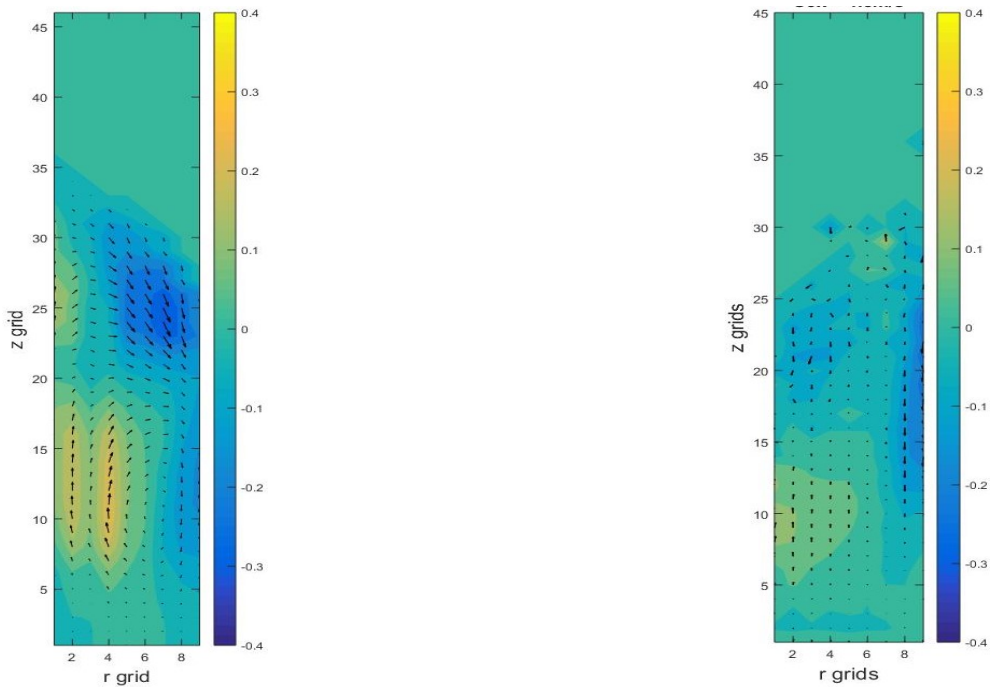


(a) Velocity profile predicted by TFM (b) Experimental velocity profile

Figure 4.21: Velocity profiles of small rods (aspect ratio=2.25) for excess velocity of 1.5m/s

However, the over prediction of bed expansion and solid velocities by the simulation especially in the case of 2.25 aspect ratio rods, could be caused because TFM does not completely account for the intense solid interactions. Although, effective restitution coefficient and frictional stress models have been incorporated in order to account for the energy loss and dynamics for dense phase regions, the closures for these models have been basically developed for nearly elastic spheres and fail when they have to take into account the non-sphericity or particle-particle entanglement that are associated with these elongated particles.

From fig4.22, we can conclude, that for the case of the 4.5 aspect ratio rods, the TFM simulation is far from predicting the actual behavior of the rods. Not only are the solid velocities and bed expansions highly over predicted, even the velocity profile obtained is not the same, i.e. the direction of granular circulation predicted by the simulation and that obtained from experiment are reversed. From the previous discussion, it is clear that the direction of granular circulation, is dependent on the inlet gas velocity and the non-sphericity of the particles. Thus, for the sake of confirmation, the simulations for the 4.5 aspect ratio rods are repeated for the excess gas velocity of 0.5m/s and 2.5m/s, which are the extreme cases considered for this study. Fig4.23 clearly shows that TFM, never predicts this reversal in flow for as it is seen in experimental case. Such deviations were also experienced by Wang et al[32], who showed that the solid circulation patterns in a fluidized bed is quite sensitive to the coefficient of restitution used. It was also demonstrated that the coefficient of restitution not only varies according to the inlet gas velocity, but also with the local solid velocities and local solid fractions, but for the current simulations a constant value of 0.97 is used. In reality, this value is quite high to describe the current system, consisting of annealed steel particles that have a rough surface and are consequently quite inelastic. This in addition to the enhanced effects of particle entanglement in the case of the 4.5 aspect ratio rods and the increased sensitivity of bubbling fluidized beds to the coefficient of restitution, when compared with a circulating fluidized bed, produces large deviations from experimental values.

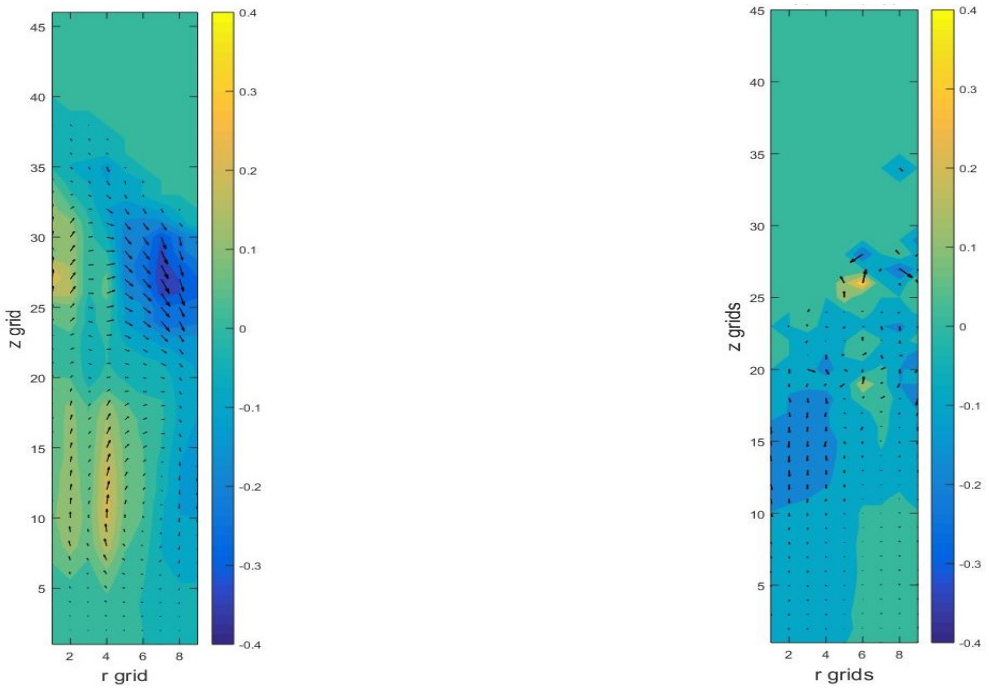


(a) Velocity profile predicted by TFM

(b) Experimental velocity profile

Figure 4.22: Velocity profiles of intermediate rods (aspect ratio=4.5) for excess velocity of 1.5m/s

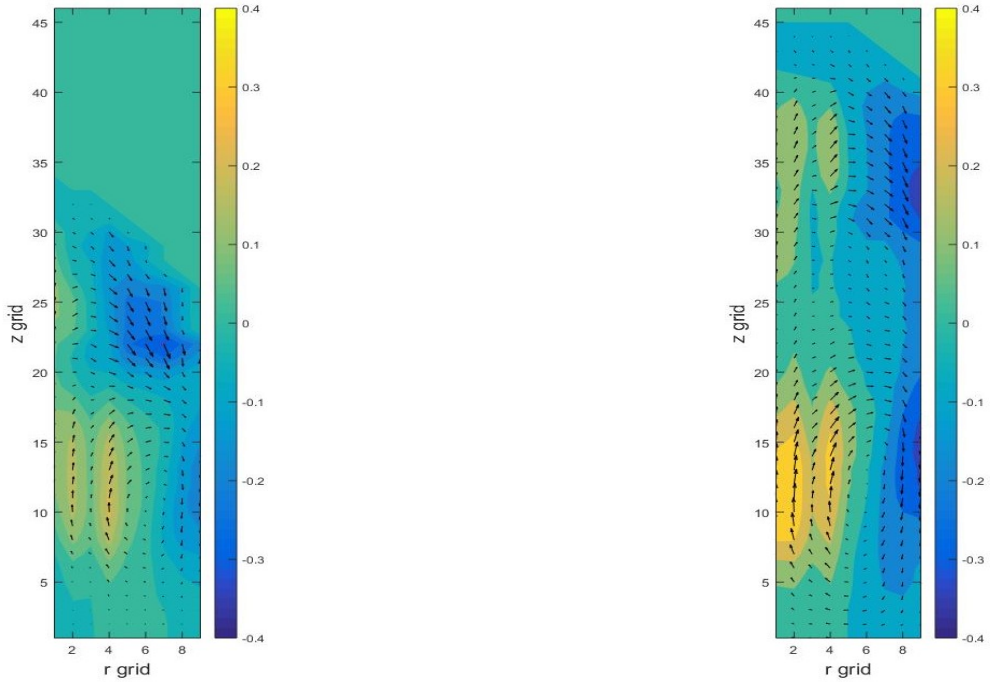


(a) Velocity profile for excess velocity of 0.5m/s

(b) Velocity profile for excess velocity of 2.5m/s

Figure 4.23: Velocity profiles predicted by TFM for intermediate rods (aspect ratio=4.5)

# Chapter 5

# Conclusions

Magnetic Particle Tracking technique is used to track the granular hydrodynamic behavior of 3 different Geldart D particles of varying aspect ratios, in a 3 Dimensional-cylindrical bubbling fluidized bed. The cylindrical particle's translational & rotational velocities, angular orientations & distributions and the local packing density in the bed were tracked and compared with the ideal case of spheres. These results were then compared with the results from the Two fluid model and the following conclusions were made:

- From the pressure drop study on the bed, it is observed that non-spherical particles have two minimum fluidization velocities owing to the presence of entanglement of these particles and that the deviation between these velocities increases with the increase in aspect ratio of the particles. The minimum fluidization velocity decreases with the increasing aspect ratio of the particle.

- With the increase in superficial gas velocity, reversal in the direction of granular circulation pattern in the bed is observed for all particles, however the velocity at which this phenomena occurs increases with the increasing aspect ratio of the cylinders. Moreover the sharpness of the transition decreases with increasing aspect ratios.

- Elongated cylinders tend to align themselves more along the flow for increasing superficial velocities. Moreover, the orientation of these cylindrical particles is not only a function of superficial velocity but also a function of its radial position in the bed.

- Rotational behavior of the spherical particles is a function of its radial position in the bed while the elongated particle exhibit no radial profile. The rotational behavior of the rods and spheres are influenced by the superficial gas velocity and it is seen that the spheres have larger mean rotational velocities than elongated particles. While the rotational behavior of spheres is strongly influenced by the granular circulation pattern, the same is not true for high aspect ratio particles.

- Spheres have higher rotational velocities at the base of the column while the rods have their maximum rotational velocities at the top of the bed, where there is less solid holdup. Thus the rotational velocity is also dependent on the axial position of the particles.

- The rotational behavior of the rods is sensitive to the amount of particles in the bed i.e.the increase in bed mass decreases the mean rotational velocity of the rods in the bed.

- The azimuthal orientation $\varphi$ of all the type of particles is independent on the superficial velocity, aspect ratio of particle and amount of particles in the bed.

- The deviation between the predictions of the Two Fluid Model and the experimental results, increases with increasing aspect ratios.

Finally it can be concluded that the Magnetic Particle Tracking technique is highly useful in qualitatively tracking several aspects of the solid phase behavior in the fluidized bed. This technique provides us with the ability to explore in detail the difference between the particles at the bulk and wall regions.

# Chapter 6

# Recommendations

Some suggestions for future work may include

1. The study of lighter non spherical particles in the fluidized bed, as the current system uses quite a heavy particle type and such heavy particles are hardly seen in industrial fluidized bed processes. Also the large density of the particles restricts the working range of superficial gas velocity, thus higher and more practical gas ranges can be used for particles with lower density.

2. Pure cylindrical particle are almost never used in industrial operations, they are always used as a mixture with other types of particle. Thus the behavior of mixtures of particles should be examined.

3. Clear difference was seen in the case of 4.5 aspect ratio rods and the spheres, however the smaller 2.5 aspect ratio rods need more study before we can definitely categorize them.

4. The sensor array of the MPT technique was quite sensitive to small power fluctuations, care should be taken to completely isolate the system or use a different sensor array before future measurement can be made.

5. Study the fluidization behavior of these non-spherical particles in a square column and compare it with the DPM simulation results.

# Bibliography


[1] J. E. Hilton, L. R. Mason, and P. W. Cleary. Dynamics of gas-solid fluidised beds with non-spherical particle geometry. *Chemical Engineering Science*, 65(5):1584–1596, 2010. 1

[2] Berend van Wachem, Marian Zastawny, Fan Zhao, and George Mallouppas. Modelling of gas-solid turbulent channel flow with non-spherical particles with large Stokes numbers. *International Journal of Multiphase Flow*, 68:80–92, 2015. 1, 4, 32

[3] Marian Zastawny, George Mallouppas, Fan Zhao, and Berend van Wachem. Derivation of drag and lift force and torque coefficients for non-spherical particles in flows. *International Journal of Multiphase Flow*, 39:227–239, 2012. 2, 3

[4] Jie Cai, Qihe Li, and Zhulin Yuan. Particuology Orientation of cylindrical particles in gas solid circulating fluidized bed. *Particuology*, 10(1):89–96, 2012. 2, 31

[5] K. B. Zitoun, S. K. Sastry, and Y. Guezennec. Investigation of three dimensional interstitial velocity, solids motion, and orientation in solid-liquid flow using particle tracking velocimetry. *International Journal of Multiphase Flow*, 27(8):1397–1414, 2001. 2, 6, 26

[6] G. Mohs, O. Gryczka, S. Heinrich, and L. Mörl. Magnetic monitoring of a single particle in a prismatic spouted bed. *Chemical Engineering Science*, 64(23):4811–4825, 2009. 2, 5, 6, 7

[7] K. Vollmari, R. Jasevičius, and H. Kruggel-Emden. Experimental and numerical study of fluidization and pressure drop of spherical and non-spherical particles in a model scale fluidized bed. *Powder Technology*, page in press, 2015. 2, 15, 26, 31

[8] J. E. Hilton and P. W. Cleary. The influence of particle shape on flow modes in pneumatic conveying. *Chemical Engineering Science*, 66(3):231–240, 2011. 2

[9] Paul W Cleary. The effect of particle shape on simple shear flows. 179:144–163, 2008. 2

[10] Paul W Cleary and Mark L Sawley. DEM modelling of industrial granular flows : 3D case studies and the effect of particle shape on hopper discharge. 26:89–111, 2002. 2

[11] M. Goldschmidt. *Hydrodynamic Modelling of Fluidised Bed Spray Granulation*. 2001. 2, 9

[12] Daizo Kunii and Octave Levenspiel. *Fluidization Engineering*. 1963. 3, 20, 26

[13] Dario Vincenzi. Orientation of non-spherical particles in an axisymmetric random flow. *Journal of Fluid Mechanics*, 719(1922):465–487, 2013. 3

[14] Matthias Mandø, Chungen Yin, Henrik Sørensen, and Lasse Rosendahl. On the modelling of motion of non-spherical particles in two-phase flow. pages 1–14, 2007. 3

[15] Shuyan Wang, Yanli Shen, Yimei Ma, Jinsen Gao, Xingying Lan, Qun Dong, and Qinglin Cheng. Study of hydrodynamic characteristics of particles in liquid-solid fluidized bed with uniform transverse magnetic field. *Powder Technology*, 245:314–323, 2013. 4

[16] Yong Zhang, Wenqi Zhong, and Baosheng Jin. Experimental investigation on the translational and rotational motion of biomass particle in a spout-fluid bed. *International Journal of Chemical Reactor Engineering*, 11(1):453–468, 2013. 4, 6, 28

[17] Wenqi Zhong, Yong Zhang, and Baosheng Jin. Novel method to study the particle circulation in a flat-bottom spout-fluid Bed. *Energy and Fuels*, 24(9):5131–5138, 2010. 5, 6

[18] Brandon S Brewster. Nonradioactive Tagging Method. 26(2):325–327, 1980. 5

[19] Stina Karlsson, Ingela Niklasson Björn, Staffan Folestad, and Anders Rasmuson. Measurement of the particle movement in the fountain region of a Wurster type bed. *Powder Technology*, 165(1):22–29, 2006. 5, 6

[20] A T Harris, J F Davidson, and R B Thorpe. A novel method for measuring the residence time distribution in short time scale particulate systems. 89:127–142, 2002. 5

[21] M K Cheezum, W F Walker, and W H Guilford. Quantitative comparison of algorithms for tracking single fluorescent particles. *Biophysical journal*, 81(4):2378–2388, 2001. 6

[22] Thomas Hagemeier, Andreas Bück, and Evangelos Tsotsas. Estimation of particle rotation in fluidized beds by means of PTV. *Procedia Engineering*, 102:841–849, 2015. 6

[23] D J Parker, T W Leadbeater, X Fan, M N Hausard, A Ingram, and Z Yang. Positron imaging techniques for process engineering: recent developments at Birmingham. *Measurement Science and Technology*, 19(9):094004, 2008. 6

[24] Maria Suzanna van Buijtenen. *Multiphase Flow in Spout Fluidized Bed Granulators*. 2011. 7

[25] K. A. Buist, T. W. van Erdewijk, N. G. Deen, and J. A M Kuipers. Determination and comparison of rotational velocity in a pseudo 2-D fluidized bed using magnetic particle tracking and discrete particle modeling. *AIChE Journal*, 61(10):3198–3207, 2015. 7, 8, 13

[26] E Stathopoulos, V Schlageter, B Meyrat, Y D E Ribaupierre, and P Kucera. Magnetic pill tracking : a novel non-invasive tool for investigation of human digestive motility. pages 148–154, 2005. 7

[27] Xuesong Lu, Chris M. Boyce, Stuart A. Scott, John S. Dennis, and Daniel J. Holland. Investigation of two-fluid models of fluidisation using magnetic resonance and discrete element simulations. *Procedia Engineering*, 102:1436–1445, 2015. 9

[28] Process Industries. Comparison of a Two-Fluid Model and an Euler-Lagrange Model for simulation of dense gas-fluidized beds. 0(December):1–6, 2015. 9

[29] Baiqian Liu, Xiaohui Zhang, Ligang Wang, and Hui Hong. Fluidization of non-spherical particles : Sphericity , Zingg factor and other fluidization parameters. 6:125–129, 2008. 17

[30] Xiao-ke Ku and Jian-zhong Lin. Motion and orientation of cylindrical and cubic particles in pipe flow with high concentration and high particle to pipe size ratio *. 9(5):664–671, 2008. 26, 29

[31] Vikrant Verma, Niels G Deen, Johan T Padding, and J A M Kuipers. Two- fluid modeling of three-dimensional cylindrical gas  solid fluidized beds using the kinetic theory of granular flow. *Chemical Engineering Science*, 102:227–245, 2013. 32

[32] Yuefa Wang, Zhongxi Chao, and Hugo A Jakobsen. A Sensitivity Study of the Two-Fluid Model Closure Parameters Determining the Main Gas - Solid Flow Pattern Characteristics. pages 3433–3441, 2010. 34

# Appendices

# Appendix A

# Supporting Studies

## A.1 Estimation of void fraction for different aspect ratio particles

To have an idea of the porosity of the bed containing these various aspect ratio particles, a simple test was done. A jar with a diameter 10 times larger than the longest axis of the particle length is selected. The particles were randomly poured into it. The volume occupied and the increase in weight of the jar was noted. Several repetitions were done and the average weight was then used to estimate the bulk density inside the jar. The porosity of the bed is then estimated using Eq A.1, neglecting the particle porosity ($\epsilon_s$) as stainless steel particles are used for this test.

$$\rho_b = \rho_s \left(1 - \epsilon_b\right) \left(1 - \epsilon_s\right) \tag{A.1}$$

Fig A.1 shows that the increase in aspect ratio of the particles increases the porosity of bed

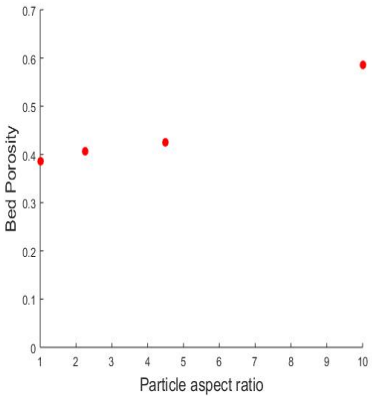


Figure A.1: Porosity of bed for different aspect ratio particles

and therefore reducing the solid holdup in the bed.

## A.2 Calculation of $u_{mf}$

The umf of the spherical particles are estimated using two methods:

**Graphical Method:**

$d_p = 0.003$m
$\rho_g = 7990 kg/m^3$

$\rho_s = 1.225kg/m^3$
$\mu_g = 1.85e^{-5}$
Estimated Dimensionless diameter

$$d_p^* = d_p \left[ \frac{\rho_g \left(\rho_s - \rho_g\right) g}{\mu_g^2} \right]^{\frac{1}{3}} = 216.33 \tag{A.2}$$

Thus $u_{mf}^*$ estimated grom graph is 2.8

$$u_{mf}^* = u \left[ \frac{\rho_g^2}{\mu_g \left(\rho_s - \rho_g\right) g} \right]^{\frac{1}{3}} \tag{A.3}$$

Thus $u_{mf}$ is estimated from the above equation is 2.76 m/s

**Using Ergun Equation**

$$\frac{1.75}{\epsilon_3^m f \phi_s} \left( \frac{d_p u_{mf} \rho_g}{\mu} \right)^2 + \frac{150 \left(1 - \epsilon_{mf}\right)}{\epsilon_m f^3 \phi_s^2} \left( \frac{d_p u_{mf} \rho_g}{\mu} \right) = \frac{d_p^3 \rho_g \left(\rho_s - \rho_g\right) g}{\mu^2} \tag{A.4}$$

The $u_{mf}$ estimated is 2.77 m/s.

## A.3 Effect of Helmholtz coil

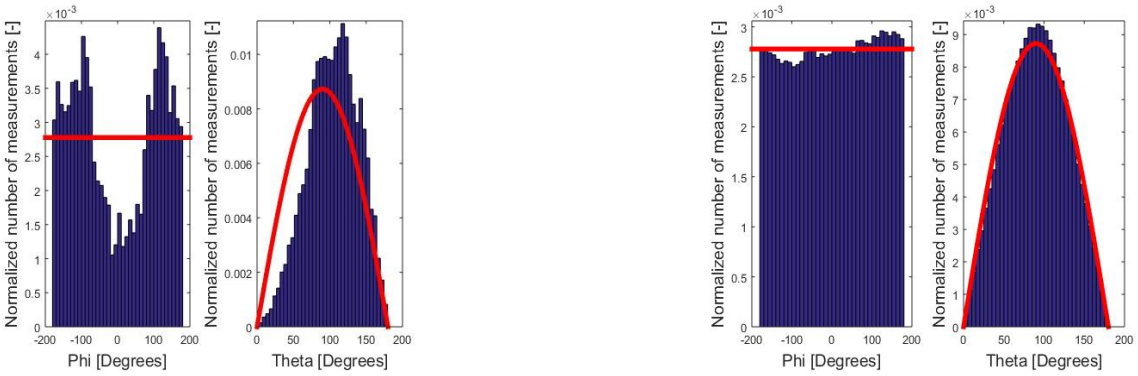


(a) Angular distribution in the absence of the Helmholtz coil

(b) Angular distribution in the presence of the Helmholtz coil

Figure A.2: Effect of Helmholtz coils for spheres

In order to visualize the role played by the Helmholtz coil, two fluidization experiments, for the same superficial velocity, one with and one without the influence of the Helmholtz coil were conducted. Since spherical particles have been studied extensively in the past and since their behavior is well know, these fluidization experiments were also carried out with spherical bed particles. The angular distribution of these experiments are shown in fig A.2a and A.2b. The azimuthal angle '$\phi$' ranging from [-180 100] is expected to have no profile within the system i.e. it is supposed to be uniformly distributed within the setup. While the angle of inclination '$\theta$' ranging from [0 180] is expected to form an half sine curve in its distribution. The red lines in these figures indicate the expected behavior of the particles and thus by comparing these two images it can be seen that the orientations of the tracer are significantly affected by the earths magnetic field. Thus confirming that it is vital to conduct the MPT experiments in a neutralized magnetic field. Moreover it was visually observed that when the Helmholtz coil was switched off the motion of the particle is not uniform throughout the bed.

## A.4 Velocity Profiles for 2.25 aspect ratio rods

The velocity profiles for the 2.25 aspect ratio rods for varying excess gas velocity examined at a bed aspect ratio of 0.5 is shown in fig A.3

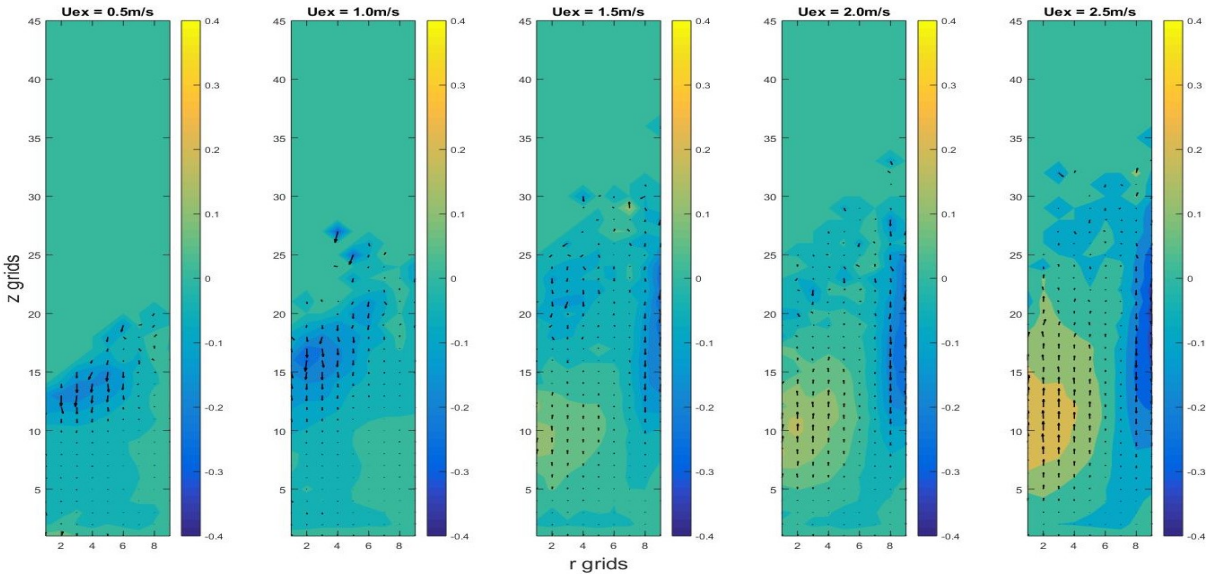


Figure A.3: Linear velocity profiles

**NOMENCLATURE**

**Roman Symbols**

| | | |
|---|---|---|
| $\overline{\overline{H}}$ | Magnetic Field | A/m |
| $\overline{e}$ | Orientational unit vector | |
| S | Sensor signal | A/m |
| $\overline{r}$ | Position vector | m |
| r | Radius | m |
| N | Number of sensors | |
| O | Occupancy of the bed | |
| P | Pressure | |
| d | Diameter | m |
| g | Acceleration due to gravity | $m/s^2$ |
| U | Velocity | m/s |
| H | Height of column | m |
| D | Diameter of column | m |
| Q | Probability function | |
| t | time | s |
| $S_p$ | Source term | N/mˆ3 |
| $\overline{u}$ | Velocity | m/s |

**Greek Symbols**

| | | |
|---|---|---|
| $\mu_m$ | Magnetic moment | $Am^2$ |
| $\mu$ | Viscosity | Kg/ms |
| $\rho$ | Density | $Kg/m^3$ |
| $\theta$ | Angle of inclination | |
| $\theta_c$ | Azimuthal angle of column | |
| $\varphi$ | Azimuthal angle of particle | |
| $\omega$ | Rotational velocity | rots/s |
| $\epsilon$ | Fraction of a phase | |
| $\tau$ | Stress tensors | $N/m^3$ |
| $\sigma$ | Standard deviation | |

**Subscripts**

| | |
|---|---|
| t | Theoretical |
| m | Measured |
| p | Particle |
| s | solid |
| g | gas |
| f | fluid |
| mf | minimum fluidization |
| x | in x-direction |
| y | in y-direction |
| z | in z-direction |
| ps | Particle to sensor |
| s | sensor |